Forward Electromagnetic Scattering Models for Sea Ice

K. M. Golden[1], M. Cheney[2], K. H. Ding[3], A. K. Fung[4], T. C. Grenfell[5], D. Isaacson[2], J. A. Kong[3], S. V. Nghiem[6], J. Sylvester[7], and D. P. Winebrenner[8]

[1]Department of Mathematics, University of Utah, Salt Lake City, Utah 84112

[2]Department of Mathematical Sciences, Rensselaer Polytechnic Institute, Troy, New York 12180

[3]Department of Electrical Engineering, Massachusetts Institute of Technology, Cambridge, Massachusetts 02139

[4]Electrical Engineering Department, University of Texas, Arlington, Texas 76019

[5]Department of Atmospheric Sciences, University of Washington, Seattle, Washington 98195

[6]Jet Propulsion Laboratory, California Institute of Technology, Pasadena, California 91109

[7]Department of Mathematics, University of Washington, Seattle, Washington 98195

[8]Applied Physics Laboratory, University of Washington, Seattle, Washington 98195

Abstract

Recent advances in forward modeling of the electromagnetic scattering properties of sea ice are presented. The results have direct relevance to microwave remote sensing, and serve as the basis for inverse algorithms for reconstructing the physical properties of sea ice from scattering data. In particular, the principal results are: (1) approximate calculations of electromagnetic scattering from multilayer random media with rough interfaces, based on the distorted Born approximation and radiative transfer theory, (2) a comprehensive theory of the effective complex permittivity of sea ice based on rigorous bounds in the quasistatic case and strong fluctuation theory in the weakly scattering regime, and (3) rigorous analysis of the Helmholtz equation and its solutions for idealized sea ice models, which has led in the one dimensional case to generalizations of classical theorems in Fourier analysis. The forward models considered here incorporate many detailed features of the sea ice system, and compare well with experimental data.

1 Introduction

Sea ice, which covers approximately 10% of the earth's ocean surface, plays a major role in the world climate system and is an indicator of global climatic change [12]. The sea ice pack forms the interface between the ocean and atmosphere in the polar regions, and mediates the exhange of heat and momentum between them. For example, the thickness and concentration of the ice are the primary factors in controlling heat exchange, with thin ice and leads playing a disproportionately large role compared to their areal extent, while surface roughness influences momentum transfer. Due to the effect of the winds and currents on the motion of the ice, the pack exhibits complex dynamical behavior. Characterizing the physical state, extent, and dynamics of the sea ice pack is a formidable problem. However, it is of clear scientific importance, as well as practical significance in navigation and in commercial, military and scientific operations in the polar regions. The sheer extent of the pack makes routine recovery of large scale information feasible only with remote sensing techniques. Due to the fact that the scattering and emission of microwaves are sensitive to the types of variations in sea ice properties which are of scientific and operational interest, microwave remote sensing offers an effective way to monitor sea ice parameters [12, 78]. Other considerations such as atmospheric transmission and ease of use on satellites, planes and ships, also contribute to the common use of frequencies in the microwave regime.

The goal of sea ice remote sensing is to use information on the electromagnetic fields scattered or emitted by the sea ice to deduce the physical properties of the pack. This is a particularly challenging problem, as sea ice is a complex, polycrystalline composite of pure ice with random brine and air inclusions, whose volume fraction and geometry depend strongly on temperature, age, and growth conditions. The surface of the ice has roughness on many scales, and is often covered with a layer of snow, which itself is another complex random composite whose microstructure can vary significantly. The layer of snow may well be infiltrated with brine or sea water. The underlying physical problem of understanding how electromagnetic waves interact with complex composite media, such as those present in the sea ice system, is of considerable interest. Due to the random nature of the variations in sea ice properties over many length scales from submillimeter to kilometers, one is usually most interested in effective electromagnetic properties obtained from ensemble or spatial averaging on an appropriate scale. Examples include the backscatter coefficient and the effective complex permittivity. Variations in such bulk coefficients are often related to variations in geophysically interesting parameters in the system.

The general problem of calculating the effective properties of random composite media has a long history, going back to early work of Maxwell [58] on the effective conductivity of a dilute suspension of spheres embedded in a host of different conductivity, and Einstein [19] on the effective viscosity of a dilute suspension of rigid spheres in a Newtonian fluid, as well as the extensive works on scattering by particles and random surfaces by Rayleigh and Kirchoff. We refer the reader to [94] and [72] for comprehensive treatments of the electromagnetic properties of various types of random media and surfaces arising in microwave remote sensing and other applications. We also note that in recent years there has been considerable attention in the physics and applied mathematics literature focused on theoretical and numerical analysis of effective, or "homogenized" coefficients of composite media [20, 55, 63, 35]. Examples of such coefficients include complex permittivity, electrical and

thermal conductivity, elastic moduli, diffusivity of turbulent fluids, and fluid permeability of porous media. Some of the methods of analysis which have received particular attention in recent years include rigorous bounds obtained from translation, variational, and complex variable methods, perturbation expansions, percolation models, and numerical algorithms such as the fast multipole method.

When electromagnetic waves interact with random media or surfaces, a key parameter determining the nature of the interaction and the types of analysis which can be used, is the ratio ξ/λ, where ξ is an appropriate measure of the length scale of variations in the medium or surface, and λ is wavelength. For example, at C-band with frequency $f = 5.3$ GHz and free space wavelength $\lambda_0 = 5.7$ cm, the wave cannot resolve the details of the brine inclusion microstructure with typical variations on a submillimeter scale, measured by ξ_{br}, with $\xi_{br} \ll \lambda_{si}$, where λ_{si} in sea ice and λ_{sn} in snow typically satisfy $\lambda_0/2 < \lambda_{si}, \lambda_{sn} < \lambda_0$. This is the so-called "quasistatic" regime, where volume scattering from individual inclusions is relatively small, and the behavior of the wave in the sea ice is determined primarily by the effective complex permittivity ϵ^* obtained from a time independent analysis, although there may be more significant scattering from larger air inclusions or grains of snow, and coherent structures such as brine drainage tubes and cracks. Surface scattering at C-band may be significant, as often there are roughness features on millimeter, centimeter and larger scales at the interfaces separating air and snow, snow and sea ice, frazil and columnar sea ice, or infiltrated and dry snow.

The electromagnetic properties of sea ice relevant to remote sensing, such as ϵ^* and the volume and surface scattering behavior, have been widely studied. The state of the art in forward microwave modeling for sea ice as of 1992 was comprehensively reviewed in [98]. Numerous approximate formulas for ϵ^* have been developed, various forms of radiative transfer theory and analytic wave theory have been applied to volume scattering in sea ice, as have numerous surface scattering models employing tangent plane approximation, perturbation, and integral equation techniques. Some electromagnetic signature models treat both surface and volume scattering, but make simplifying assumptions about interactions between the two types. All of these models are based on Maxwell's equations for linear, non-magnetic media, but differ in the types of approximations made, in how the medium is characterized, and in applicability to different frequency regimes.

While much progress was made in the twenty years or so prior to 1992 in modeling the electromagnetic properties of sea ice, there has remained a large gap in how our understanding of forward electromagnetic modeling could be used to quantitatively recover sea ice parameters of geophysical, climatological and operational interest via remote sensing techniques. In an effort to fill this gap, a five year Accelerated Research Initiative (ARI) on Sea Ice Electromagnetics, sponsored by the Office of Naval Research, was begun in 1992. The initiative was interdisciplinary in nature, involving over 60 researchers at 20 institutions, and consisted of three closely integrated components: modeling, and laboratory and field experiments. The prinicpal goals of the ARI were to improve our understanding of how the physical properties of sea ice determine its electromagnetic behavior, and in turn, to use this knowledge to develop and test inverse algorithms for recovering sea ice parameters from observed electromagnetic data. A key step in accomplishing these goals is further development of forward models of the electromagnetic properties of complex media, and sea ice in particular. This paper gives an overview of our main results on the forward problem. How

these models are used to develop inverse algorithms is presented in [34]. What particularly distinguished the ARI from previous efforts has been (*i*) the integration of model development with laboratory experiments designed to test and help refine the models, (*ii*) the focus on the development of **inverse** algorithms, and (*iii*) recent advances in the mathematical theories of electromagnetic inverse scattering and homogenization for composite materials have been brought to bear on the problem of sea ice remote sensing, which in turn has led to new theoretical findings. From a forward modeling perspective, our principal contributions include the following:

- Significant refinement of approximate calculations of electromagnetic scattering from sea ice based on the distorted Born approximation, strong fluctuation theory, and radiative transfer theory. Model improvement was accomplished through close integration with experiments, incorporation of realisistic features of the sea ice system, and accounting for both volume and surface scattering.

- Rigorous, mathematical analysis of the forward electromagnetic scattering problem and its solutions for an idealized sea ice system, treated as a one dimensional layered medium, and an inhomogeneous, dissipative half-space in three dimensions. Surprising generalizations of classical theorems in Fourier analysis were obtained from the layered medium theory.

- Comprehensive theory of the effective complex permittivity ϵ^* of sea ice, and how it is determined by the microstructural characteristics. Rigorous bounds on ϵ^* valid in the quasistatic regime were obtained using an analytic continuation method, and an approximate model based on strong fluctuation theory, which incorporates scattering effects at higher frequencies and many detailed features of the sea ice microstructure, was also developed.

The paper is organized as follows. In sections 2 and 3 we present rigorous, general results on the forward problem for idealized models of sea ice. In sections 4 and 5 we focus on approximate methods of calculating the scattering properties of multilayer, random media models for sea ice. These results form the basis for the inverse algorithms in [34].

The main results considered here are summarized as follows. In section 2, the Helmholtz equation with an index of refraction varying in one dimension (neglecting dissipation) is analyzed through the introduction of "travel-time coordinates" [89]. An analog of the Plancherel equality in Fourier analysis, which states that the "energy" (or L^2 norm) of a function is preserved under Fourier transform, is obtained. In particular, an equality relating appropriate energies for the reflection coefficient in the frequency domain and for the variation in the index of refraction, which reduces to the classical Plancherel equality in the limit of small variations, has been discovered. While Fourier analysis can be viewed as spectral theory for the Helmholtz equation in a homgeneous medium, this new work can be viewed as generalizing such ideas to inhomogeneous media. Subsequently, the Helmholtz equation with complex index of refraction (including dissipation) varying in a half-space in three dimensions is analyzed [13]. Through conversion of the differential equation to an integral equation (with a Green's function kernel) that incorporates the boundary conditions at infinity, solutions to the forward scattering problem can be constructed. A rigorous theorem establishing existence and uniqueness is obtained.

In section 3 we present a series of rigorous bounds on the quasistatic permittivity ϵ^* of sea ice, treated as a general two component random medium [27, 77, 31]. These bounds restrict ϵ^* to increasingly smaller regions of the complex ϵ^*-plane as one knows more information about the microstructure, such as the brine volume and geometry, and represent an alternative to the wide variety of approximate mixing formulas which have been applied to sea ice. The bounding procedure exploits the properties of ϵ^* as an analytic function of the ratio of the component permittivities, and is based on a Stieltjes integral representation for ϵ^* involving the spectral measure of a self-adjoint operator associated with the geometry of the microstructure. Particularly tight bounds are obtained when one further imposes the condition that the brine phase is contained in separated inclusions. This "matrix-particle" structure forces a gap in the spectrum, with colder temperatures corresponding to greater separation, a larger gap, and tighter bounds. Such bounds are valid up to the critical brine volume fraction $p_c \approx 5\%$, or percolation threshold, above which the brine phase is connected on a macroscopic scale, and the sea ice is permeable to fluid transport.

The above bounds apply to wave propagation in the quasistatic regime. However, as frequency or inclusion size is increased, scattering effects become more significant. Two principal approaches have been used to deal with the problem of incorporating scattering effects: wave theory and radiative transfer theory [94]. In analytic wave theory, approximate solutions to the vector wave equation arising from Maxwell's equations, such as the Born, or first order approximation, are used to estimate the scattering characteristics of the medium. Radiative transfer theory, on the other hand, begins not with Maxwell's equations but with the radiative transfer equation governing the propagation of energy through the scattering medium. While this theory is heuristic, it is simpler than analytic wave theory and incorporates multiple scattering effects. In section 4 we consider analytic wave theory for a multilayer, anisotropic, random medium model of sea ice with rough interfaces, which incorporates detailed properties of the brine, air, crystallographic, and snow microstructures [67, 70]. In particular, the distorted Born approximation is used in conjuction with strong fluctuation theory to calculate the scattering characteristics. This approximation for the incoherent scattered field incorporates single scattering of the coherent field, whose propagation characteristics are assumed determined by the effective complex permittivity. For media with strong permittivity fluctuations such as sea ice, this effective complex permittivity, including scattering effects, is approximated with strong fluctuation theory [66, 70, 94]. Finally in section 5 we consider radiative transfer theory for a similar, multilayer random inclusion model of sea ice. A schematic representation of such a model is shown in Figure 1.

2 Forward scattering theory for the Helmholtz equation

In this section we formulate the forward scattering problem for the Helmholtz equation for idealized sea ice models, and give general properties of its solutions. These results lay the groundwork for the advances in inverse scattering theory discussed in [34]. The sea ice scattering problem can be modeled as a half-space problem in $\mathbf{R}^d$, where measurements are made in the upper half-space, which is homogeneous and non-dissipative, while the lower half-space is inhomogeneous and dissipative. We consider an electromagnetic wave of a particular frequency in such a medium (assumed non-magnetic), whose time-harmonic

electric field is given by $\mathbf{E}(\mathbf{x},t) = \mathbf{E}(\mathbf{x})e^{-i\omega t}, \mathbf{x} \in \mathbf{R}^d$ (with $\mathbf{x} = (x_1, x_2, x_3)$ in $d = 3$), $t \in \mathbf{R}$, with $\omega = 2\pi f$ and f the frequency in Hz. The relative complex permittivity $\epsilon(\mathbf{x})$ of the medium, assumed isotropic, is given by $\epsilon = \epsilon_r/\epsilon_0 + i\sigma/(\omega\epsilon_0)$, where ϵ_r is the (real) permittivity, ϵ_0 is the permittivity of free space, and σ is the conductivity. In the upper half space occupied by air, $\epsilon = 1$, with zero imaginary part. In the lower half space occupied by sea ice, snow, and sea water, $\epsilon(\mathbf{x})$ takes a wide range of values, often with large imaginary part, in the various media that are encountered, such as pure ice, brine, air, fresh water and sea water. The electric field $\mathbf{E}(\mathbf{x},t)$ satisfies Maxwell's equations, or the classical wave equation derived from them. Under the time-harmonic assumption, the cartesian components of spatial part $\mathbf{E}(\mathbf{x})$ of the electric field, represented by a general wave field u, satisfy the Helmholtz equation

$$\nabla^2 u + k^2 \tilde{\epsilon} u \doteq 0, \tag{2.1}$$

where k is the free space wave number $k = \omega\sqrt{\mu_0\epsilon_0} = \omega/c$, μ_0 is the magnetic permeability of free space, and c is the velocity of light in free space. In what follows it will be useful in (2.1) to write $k^2\epsilon = k^2n^2 + ikm$, where $n = \sqrt{\epsilon_r/\epsilon_0}$ is the index of refraction, and $m = \sigma\sqrt{\mu_0/\epsilon_0}$. Equation (2.1) can be thought of as a scalar model for electromagnetic wave propagation. It is simpler than the full Maxwell's equations but it retains the key mechanisms of variable speed of propagation and dissipation. Equation (2.1) also governs acoustic wave propagation.

2.1 Layered media

Of significant interest in many geophysical contexts is the Helmholtz equation for layered media, where $\epsilon(\mathbf{x})$ in the lower half-space varies only in the vertical, or depth variable $z = x_3$. For simplicity, we explicitly consider here only the vertical incidence problem for reflection off the lower half-space $z < 0$, yielding a one dimensional problem, while noting that it is straightforward to extend the results to off-nadir reflection at either vertical or horizontal polarization. The following analysis serves as the basis for a causally stabilized layer stripping algorithm [89, 34] developed to reconstruct the index of refraction at progressively increasing depths in the reflecting medium. The results have been rigorously established for the case of wave propagation in a system governed by the Helmholtz equation without loss ($\sigma = 0$) and without discontinuities in the dielectric properties. Nevertheless, computational evidence shows that simple modifications of the same results provide usefully approximate solutions in problems including both dielectric jumps and loss typical of sea ice. In the following, we summarize the forward scattering problem and an analog, for the reflection problem, of the Plancherel equality in linear Fourier analysis.

The Helmholtz equation governing the time-harmonic wave field u in one dimension, assuming sources only at infinity, is

$$\frac{d^2u}{dz^2} + k^2n^2(z)u = 0. \tag{2.2}$$

We assume that the (dimensionless and, for now, real) index of refraction, n, differs from 1 only on the interval $(-\infty, 0)$, and that $\frac{d}{dz}\frac{1}{\sqrt{n}}$ is square-integrable on that interval. It is

well-known that there is a unique solution to equation (2.2) that is down-going at infinite depth.

Analysis of both the forward and inverse problems is facilitated by the introduction of so-called travel-time coordinates. Define a new "depth" variable x by the relation

$$x(z) \equiv \int_0^z n(\tau) d\tau. \tag{2.3}$$

Because n is real and positive, x is an invertible function of z. Define $v(x) \equiv u(z(x))$, $\gamma(x) \equiv n(z(x))$, and finally

$$\alpha(x) \equiv \frac{1}{\gamma(x)} \frac{d\gamma}{dx}. \tag{2.4}$$

Note that v is actually a function of k as well as x. If we know $\alpha(x)$ we can solve (2.4) for $\gamma(x)$ using the boundary condition at $\gamma(0) = 1$; then with γ we can solve the differential equation (with its boundary condition) implied by (2.3). Note that $\alpha(x) = 0$ for $x \geq 0$. A little manipulation shows that v satisfies

$$v'' + \alpha v' + k^2 v = 0, \tag{2.5}$$

where the primes denote differentiation with respect to x, and where the condition that we seek solutions down-going at infinite depth takes the form $v \sim e^{-ikx}$ as $x \to -\infty$.

For $x > 0$, $v(x,k)$ may be written in the form

$$v(x,k) = \frac{1}{T(k)} \left[e^{-ikx} + R(k) e^{ikx} \right], \tag{2.6}$$

which uniquely defines the reflection coefficient, $R(k)$. Knowledge of $R(k)$ at all values of k completely determines $\alpha(x)$, and thus $n(z)$, in principle. The additional requirements that the time-domain impulse response of the reflecting medium be real and causal, i.e., that there can be no response prior to excitation, force $R(-k) = \overline{R(k)}$, for k on the real axis, where the overbar denotes complex conjugation, and $R(k)$ to extend analytically to the upper half of the complex k-plane.

Equation (2.6) represents the wavefield above the reflecting medium in terms of reflected and incident plane waves. There is no similar representation at depths (inside the reflecting medium) at which $\alpha \neq 0$. However, defining

$$\eta \equiv \frac{v'(x,k)}{-ikv(x,k)} \tag{2.7}$$

and

$$r(x,k) \equiv \frac{1-\eta}{1+\eta} \tag{2.8}$$

gives us a "depth-dependent reflection coefficient" $r(x,k)$, such that $r(0,k) = R(k)$ and r has the physical meaning of a reflection coefficient (in the sense of (2.6)) anywhere that $\alpha = 0$.

Our first result [89] is a precise characterization of $R(k)$ and $r(x,k)$, and takes the form of a Plancherel-like equality. Any square-integrable $\alpha(x)$ gives rise to an $R(k)$ with magnitude

less than 1 at all k, which satisfies the symmetry and analyticity conditions stated above, and for which

$$\mathcal{E}(R) \equiv -\int_{-\infty}^{\infty} \log(1-|R(k)|^2)dk < \infty. \tag{2.9}$$

In fact,

$$\mathcal{E}(R) = \frac{\pi}{16}\int_{-\infty}^{0}\left|\frac{d}{dz}\frac{.1}{\sqrt{n(z)}}\right|^2 dz = \frac{\pi}{4}\int_{-\infty}^{0}|\alpha(x)|^2 dx. \tag{2.10}$$

Moreover, any complex function $R(k)$ with the stated analyticity and symmetry, and with finite "energy" $\mathcal{E}(R)$, corresponds to some square-integrable profile $\alpha(x)$. The "energy" can be computed from the data or from the profile using equations (2.9) or (2.10), respectively. A similar relation holds involving the depth-dependent reflection coefficient:

$$\mathcal{E}(r(x_1,\cdot)) - \mathcal{E}(r(x_0,\cdot)) = \frac{\pi}{4}\int_{x_1}^{x_0}|\alpha(x)|^2 dx. \tag{2.11}$$

We refer to equation (2.10) as a Plancherel-like equality because it reduces to precisely the Plancherel equality in the limit of small α, and thus small reflection. Equation (2.11) is useful as a diagnostic in numerical computations to solve both the forward and inverse problems.

2.2 Perturbed dissipative half-space

We now consider the forward scattering theory for (2.1) with dissipation,

$$\nabla^2 u + (k^2 n^2 + ikm)u = 0, \tag{2.12}$$

in the case where $n = 1, m = 0$ for $x_3 \geq 0$, while in the lower half-space $x_3 < 0$, n differs from a positive constant n_- only in a region of compact support, and m differs from a positive constant m_- only in this region as well [13]. These assumptions are meant to include the case of an ice floe in sea water. For simplicity we assume that the medium is unchanging in the x_2 direction, so that we need consider only the transverse electric polarization, and then u in (2.12) represents E_2, the component of the electric field $\mathbf{E}$ in the x_2 direction, and the Laplacian ∇^2 is two-dimensional in the x_1 and x_3 variables. A number of references on the theory of scattering from a half-space in the non-dissipative case, for layered media, and more general situations, are given in [13].

For any incident field, solutions to the direct scattering problem can be constructed in the usual way by converting the differential equation (2.12) to an integral equation that builds in the boundary conditions at infinity. The kernel of this integral equation is a Green's function for the unperturbed problem with outgoing boundary conditions. In particular, this Green's function is

$$G_0(\mathbf{x},\mathbf{y}) = \frac{1}{(2\pi)^2}\int e^{i(\mathbf{x}'-\mathbf{y}')\cdot\mathbf{k}'}\hat{G}_0(\mathbf{k}', x_3, y_3)d\mathbf{k}', \tag{2.13}$$

where $\mathbf{x}' = (x_1, x_2)$ and $\mathbf{y}' = (y_1, y_2)$, the hat denotes two dimensional Fourier transform in x_1 and x_2, and with the notation $\lambda_+ = \sqrt{k^2 - |\mathbf{k}'|^2}$, $\lambda_- = \sqrt{-|\mathbf{k}'|^2 + k^2 n_-^2 + ikm_-}$,

$$\hat{G}_0(\mathbf{k}', x_3, y_3) = \frac{i}{2\lambda_+}\begin{cases} R(\lambda_+,\lambda_-)e^{i\lambda_+(x_3+y_3)} + e^{i\lambda_+|x_3-y_3|}, & \text{for } x_3 > 0 \\ T(\lambda_+,\lambda_-)e^{i\lambda_+ y_3}e^{-i\lambda_- x_3}, & \text{for } x_3 < 0 \end{cases} \tag{2.14}$$

for the case when $y_3 > 0$ and

$$\hat{G}_0(\mathbf{k}', x_3, y_3) = \frac{i}{2\lambda_-} \begin{cases} T(\lambda_-, \lambda_+) e^{-i\lambda_- y_3} e^{i\lambda_+ x_3}, & \text{for } x_3 > 0 \\ e^{i\lambda_- |x_3 - y_3|} + R(\lambda_-, \lambda_+) e^{-i\lambda_-(x_3+y_3)}, & \text{for } x_3 < 0 \end{cases} \tag{2.15}$$

for the case when $y_3 < 0$, where

$$T(\lambda_1, \lambda_2) = \frac{2\lambda_2}{\lambda_1 + \lambda_2} \tag{2.16}$$

and

$$R(\lambda_1, \lambda_2) = \frac{\lambda_2 - \lambda_1}{\lambda_1 + \lambda_2}. \tag{2.17}$$

Note that since the imaginary parts of λ_+ and λ_- are nonnegative, the exponents in (2.14) and (2.15) are decaying.

For an incident wave E^i, a **scattering solution** E of (2.12) can be constructed as the solution to the integral equation

$$E(\mathbf{x}) = E^i(\mathbf{x}) + \int G_0(\mathbf{x}, \mathbf{y}) V(\mathbf{y}) E(\mathbf{y}) d\mathbf{y}, \tag{2.18}$$

where we have written $V(\mathbf{y}) = k^2(n^2(\mathbf{y}) - n_-^2) + ik(m(\mathbf{y}) - m_-)$. The scattering solution $G(\mathbf{x}, \mathbf{y})$ at $\mathbf{x}$ due to a point source at $\mathbf{y}$ should satisfy the resolvent equation

$$G(\mathbf{x}, \mathbf{y}) = G_0(\mathbf{x}, \mathbf{y}) + \int G_0(\mathbf{x}, \mathbf{z}) V(\mathbf{z}) G(\mathbf{z}, \mathbf{y}) d\mathbf{z}. \tag{2.19}$$

The Green's function G, however, has a singularity at $\mathbf{x} = \mathbf{y}$, which causes some technical problems. We therefore write the resolvent equation in terms of the scattered wave G_s, which is defined by $G = G_0 + G_s$,

$$G_s = \int G_0 V G_0 + \int G_0 V G_s \, . \tag{2.20}$$

It has been shown [13] that both equations have unique solutions in the space $H^{1,q}$, for any $q > 1/2$, where

$$H^{1,q} = \{u : D^\alpha u \in L^{2,q}, |\alpha| \leq 1\}, \tag{2.21}$$

and

$$L^{2,q}(\mathbf{R}^3) = \{u : (1 + |x_3|^2)^{q/2} u \in L^2(\mathbf{R}^3)\}. \tag{2.22}$$

A boundary value problem can be defined by (2.12) for $x_3 < 0$ with the boundary condition $u|_{x_3=0} = f$, together with an outgoing radiation condition in the lower half-space. If f is in the Sobolev space $H^{1/2}$ and $m > 0$, the Lax-Milgram theorem can be used to show that this boundary value problem has a unique H^1 solution in the lower half-space. Thus the normal derivative $\partial u / \partial \nu$ on the surface $x_3 = 0$ is uniquely determined. The mapping from $H^{1/2}$ to $H^{-1/2}$

$$\Lambda : u|_{x_3=0} \mapsto \frac{\partial u}{\partial \nu}|_{x_3=0} \tag{2.23}$$

is called the Dirichlet-to-Neumann map. Such maps have been used a great deal recently in the study of inverse problems, for example in [88, 79].

3 Bounds on the quasistatic effective complex permittivity

We continue our presentation of rigorous results for the forward problem by considering the complex permittivity of sea ice. Due to the wide range of relevant sea ice microstructures, as well as the high dielectric contrast of its components, it is in general quite difficult to accurately predict the effective complex permittivity ϵ^* of sea ice, even in the quasistatic limit where scattering effects are negligible. Nevertheless, many models have been developed, where typically the sea ice is assumed to be a pure ice host with ellipsoidal brine and air inclusions. Various effective medium theories, such as the coherent potential approximation, have been used to derive "mixing formulas" for ϵ^*. A survey of such results is contained in [39]. While mixing formulas are certainly useful, their applicability to the full range of sea ice microstructures is questionable, as the geometrical assumptions inherent in the formulas are often not satisfied. Furthermore, they do not readily provide information on the *range* of reasonable values for ϵ^*, corresponding to natural variations in the microstructural characteristics. In view of these limitations for mixing formulas, a new approach to predicting the effective complex permittivity of sea ice has been developed. A general, analytic continuation method for obtaining rigorous bounds on effective parameters of composite media [5, 59, 28] has been applied to sea ice [27]. Accounting for the matrix-particle (or host-inclusion) structure of sea ice has led to advances in the method and to much tighter bounds [77, 31], which have also been applied to some smart materials consisting of an insulating matrix with conducting particles [30]. We remark that the series of bounds considered here forms the basis of an inversion scheme for reconstructing the brine volume and other microstructural characteristics from data on ϵ^* [14, 34].

It should be noted that the analytic continuation method, which exploits Stieltjes integral representations for the effective parameters, has been used in a variety of contexts, including bounds on dispersion implied by finite frequency-range Kramers Kronig relations [61], and the effective diffusivity of tracers in a turbulent fluid [3]. Recently, we have used the Stieltjes properties of effective transport coefficients to establish a rigorous connection between phase transitions in statistical mechanics, and the transition in transport properties that occurs at a percolation threshold [29], such as that exhibited by sea ice at its critical brine volume fraction $p_c \approx 5\%$.

Let us now describe the analytic continuation method, and how it is used to obtain bounds on the complex permittivity of sea ice. Consider a two phase random medium in all of $\mathbf{R}^d$, with an isotropic local complex permittivity $\epsilon(\mathbf{x}, \beta)$, taking values ϵ_1 and ϵ_2, the permittivities of brine and ice, respectively, with $\epsilon(\mathbf{x}, \beta)$ a stationary random field in $\mathbf{x} \in \mathbf{R}^d$ and $\beta \in \Omega$, where Ω is the set of all realizations of the random medium. We write $\epsilon(\mathbf{x}, \beta) = \epsilon_1\chi_1(\mathbf{x}, \beta) + \epsilon_2\chi_2(\mathbf{x}, \beta)$, where χ_j is the characteristic function of medium $j = 1, 2$, which equals one for all realizations $\beta \in \Omega$ having medium j at $\mathbf{x}$, and equals zero otherwise. Let $\mathbf{E}(\mathbf{x}, \beta)$ and $\mathbf{D}(\mathbf{x}, \beta)$ be the stationary random electric and displacement fields, related by $\mathbf{D} = \epsilon\mathbf{E}$, satisfying

$$\nabla \cdot \mathbf{D} = 0, \qquad \nabla \times \mathbf{E} = \mathbf{0}, \tag{3.1}$$

where $\langle \mathbf{E}(\mathbf{x}, \beta) \rangle = \mathbf{e}_k$, $\mathbf{e}_k$ is a unit vector in the k^{th} direction, for some $k = 1, \ldots, d$, and $\langle \cdot \rangle$ means ensemble average over Ω or spatial average over all of $\mathbf{R}^d$. The effective complex

permittivity tensor ϵ^* is defined as

$$\langle \mathbf{D} \rangle = \epsilon^* \langle \mathbf{E} \rangle. \tag{3.2}$$

For simplicity, we focus on one diagonal coefficient $\epsilon^* = \epsilon^*_{kk}$. Due to homogeneity of effective parameters, $\epsilon^*(a\epsilon_1, a\epsilon_2) = a\epsilon^*(\epsilon_1, \epsilon_2)$ for any constant a, ϵ^* depends only on the ratio $h = \epsilon_1/\epsilon_2$, and we define $m(h) = \epsilon^*/\epsilon_2$. The two main properties of $m(h)$ are that it is analytic off $(-\infty, 0]$ in the h–plane, and that it maps the upper half plane to the upper half plane, so that it is an example of a Stieltjes, or Herglotz function.

The key step in the analytic continuation method is obtaining an integral representation for ϵ^*. For this purpose it is more convenient to consider $F(s) = 1 - m(h), s = 1/(1-h)$, which is analytic off $[0,1]$ in the s–plane [4]. Then [28]

$$F(s) = 1 - \frac{\epsilon^*}{\epsilon_2} = \int_0^1 \frac{d\mu(z)}{s - z}, \qquad s = \frac{1}{1 - \epsilon_1/\epsilon_2}, \tag{3.3}$$

where μ is a positive measure on $[0,1]$. This formula is essentially a spectral representation of the resolvent $\mathbf{E} = (s + \Gamma\chi_1)^{-1}\mathbf{e}_k$, obtained from (3.1) and (3.2), where $\Gamma = \nabla(-\Delta)^{-1}\nabla\cdot$, $\Delta = \nabla^2$ and in Γ, $(-\Delta)^{-1}$ is convolution with the free-space Green's function for $-\Delta$. In the Hilbert space $L^2(\Omega, P)$ with weight χ_1 in the inner product, $\Gamma\chi_1$ is a bounded self adjoint operator with norm ≤ 1. In (3.3), μ is a spectral measure of $\Gamma\chi_1$. One of the most important features of (3.3) is that it separates the parameter information in s or h from information about the geometry of the mixture, which is all contained in μ.

Statistical assumptions about the geometry are incorporated into μ through its moments μ_n. Comparison of the perturbation expansion of (3.3) around a homogeneous medium ($s = \infty$, or $\epsilon_1 = \epsilon_2$),

$$F(s) = \frac{\mu_0}{s} + \frac{\mu_1}{s^2} + \frac{\mu_2}{s^3} + \ldots, \tag{3.4}$$

with a similar expansion of the resolvent representation for $F(s)$ [28], yields

$$\mu_n = \int_0^1 z^n d\mu(z) = (-1)^n \langle \chi_1 [(\Gamma\chi_1)^n e_k] \cdot e_k \rangle. \tag{3.5}$$

Then $\mu_0 = p_1$ if only the volume fractions p_1 and $p_2 = 1 - p_1$ are known, and $\mu_1 = p_1 p_2/d$ if the material is statistically isotropic. In general, knowledge of the $(n+1)$–point correlation function of the medium allows calculation of μ_n (in principle). Expansion (3.4) converges only in the disc $|h - 1| < 1$, and the integral representation (3.3) provides the **analytic continuation** of (3.4) to the full domain of analyticity. In this way, information obtained about a nearly homogeneous system can be used, remarkably, to analyze the system near percolation as $h \to 0$ or $h \to \infty$.

Bounds on ϵ^*, or $F(s)$, are obtained by fixing s in (3.3), varying over admissible measures μ (or admissible geometries), such as those that satisfy only $\mu_0 = p_1$, and finding the corresponding range of values of $F(s)$ in the complex plane. Two types of bounds on ϵ^* are readily obtained. The first bound R_1 assumes only that the relative volume fractions p_1 and $p_2 = 1 - p_1$ are known, so that only $\mu_0 = p_1$ need be satisfied. In this case, the admissible set of measures forms a compact, convex set. Since (3.3) is a linear functional of μ, the extreme values of F are attained by extreme points of the set of admissible measures,

which are the Dirac point measures of the form $p_1\delta_z$. The values of F must lie inside the circle $p_1/(s-z)$, $-\infty \le z \le \infty$, and the region R_1 is bounded by circular arcs, one of which is parametrized in the F–plane by

$$C_1(z) = \frac{p_1}{s-z}, \qquad 0 \le z \le p_2. \tag{3.6}$$

To obtain the other arc, it is convenient to use the auxiliary function [6] $E(s) = 1 - \epsilon_1/\epsilon^* = (1-sF)/(s(1-F))$, which is a Stieltjes function like $F(s)$, analytic off $[0,1]$, with a representation like (3.3) whose representing measure has mass p_2. Then in the E–plane, the other circular boundary of R_1 has a parameterization similar to (3.6). In the ϵ^*–plane, R_1 has vertices $(p_1/\epsilon_1 + p_2/\epsilon_2)^{-1}$ and $p_1\epsilon_1 + p_2\epsilon_2$, and collapses to the interval $(p_1/\epsilon_1 + p_2/\epsilon_2)^{-1} \le \epsilon^* \le p_1\epsilon_1 + p_2\epsilon_2$ when ϵ_1 and ϵ_2 are real, which are the classical arithmetic (upper) and harmonic (lower) mean bounds, also called the elementary bounds.

If the material is further assumed to be statistically isotropic, i.e., $\epsilon^*_{ik} = \epsilon^*\delta_{ik}$, then $\mu_1 = p_1p_2/d$ must be satisfied as well. A convenient way of including this information is to use the transformation [6, 26] $F_1(s) = 1/p_1 - 1/(sF)$. The function $F_1(s)$ is, again, a Stieltjes function having a representation like (3.3) with representing measure μ^1, with only a restriction on its mass $\mu^1_0 = p_2/p_1d$. Applying the same procedure as for R_1 yields a region R_2, whose boundaries are again circular arcs. In the ϵ^*–plane, R_2 has vertices which collapse to the interval

$$\epsilon_2 + p_1\left(\frac{1}{\epsilon_1-\epsilon_2} + \frac{p_2}{d\epsilon_2}\right)^{-1} \le \epsilon^* \le \epsilon_1 + p_2\left(\frac{1}{\epsilon_2-\epsilon_1} + \frac{p_1}{d\epsilon_1}\right)^{-1}, \tag{3.7}$$

when ϵ_1 and ϵ_2 are real with $\epsilon_1 \ge \epsilon_2$, which are the famous Hashin–Shtrikman bounds [40]. We remark that higher–order correlation information can be conveniently incorporated by iterating the above transformation, as in [26].

As mentioned above, tighter bounds on ϵ^* can be obtained if the material has a matrix-particle structure with separated inclusions. In this case, the support of μ in (3.3) lies in an interval $[s_m, s_M]$, $0 < s_m < s_M < 1$, as observed in fundamental work by Bruno [11]. The further the separation of the inclusions, the smaller the support interval $[s_m, s_M]$, and the tighter the bounds. We will indicate later how these values of s_m and s_M are chosen for relevant microgeometries. A convenient way of incorporating the support restriction is to first consider a new variable t, defined by $s = (s_M - s_m)t + s_m$. Then the interval $[s_m, s_M]$ in the s–plane gets mapped to $[0,1]$ in the t–plane, and the function $H(t) = F(s) = F((s_M - s_m)t + s_m)$ is analytic off $[0,1]$ in the complex t–plane. Then there is a positive measure ν on $[0,1]$ such that

$$H(t) = \int_0^1 \frac{d\nu(z)}{t-z}. \tag{3.8}$$

With $\Lambda = s_M - s_m$ the spectral width, it can be shown that $\nu_0 = p_1/\Lambda$ if only the volume fractions are known, and $\nu_1 = \frac{p_1}{\Lambda^2}\left(\frac{p_2}{d} - s_m\right)$ if the material is statistically isotropic. While the details become somewhat involved, bounds on ϵ^* are obtained through a similar extremal procedure to that outlined above applied to $H(t)$ and its auxiliary functions. If just the volume fractions are assumed, then we obtain for matrix-particle composites a region R_1^{mp} in the complex ϵ^*–plane, and if the medium is further assumed to be statistically isotropic,

we obtain a region R_2^{mp}. R_1^{mp} and R_2^{mp} provide improvements over the complex elementary and Hashin-Shtrikman bounds R_1 and R_2. We refer the reader to [31] for the details.

In order to illustrate the above series of bounds, we briefly describe how to compare them with data in [2]. Given a sea ice sample of temperature $T°C$ and salinity S parts per thousand (ppt), the brine volume p_1 is calculated from the equation of Frankenstein and Garner [22]. Given the frequency f GHz as well, the complex permittivity ϵ_1 of the brine is computed from the equations of Stogryn and Desargant [86]. Furthermore, although the brine microstructure tends to be elongated in the vertical direction, since only vertically incident waves are considered in [2], we assume that the geometry is isotropic within the horizontal plane, in which case we take $d = 2$ above. (Marked anisotropy within the horizonal plane in the presence of a well defined current direction during growth was considered in [32].) While the sea ice is actually a three component medium, we have found that very close agreement of the two component bounds with the data can be obtained [14, 31] if we slightly adjust the complex permittivity ϵ_2 of the ice by treating it as a composite with a small volume fraction of air, and calculating its effective permittivity ϵ_2 with the Maxwell–Garnett formula,

$$\epsilon_2 = \epsilon_{ice}\left[1 - \frac{d\, p_{air}(\epsilon_{ice} - \epsilon_{air})}{\epsilon_{ice}(d-1) + \epsilon_{air} + p_{air}(\epsilon_{ice} - \epsilon_{air})}\right], \tag{3.9}$$

where $\epsilon_{ice} = (3.1884 + 0.00091\ T) + i\ 0.00005$ [57], $\epsilon_{air} = 1$, $d = 3$, and p_{air}, air volume fraction, is calculated via the equations in [16] from the density of the sample, T and S. It should be remarked that the three component case can also be treated with the multi-component bounds obtained in [26, 60, 62], although the mathematics involves holomorphic functions of several complex variables, and is quite a bit deeper than the two component case, with a number of unresolved issues.

Finally, to compare the data with our matrix-particle bounds, we assume that within the horizontal plane, the brine is contained in separated, circular discs, which allows us to utilize the explicit calculations in [11] of s_m and s_M. In particular, we consider discs of brine of radius r_b which hold random positions in a host of ice, in such a way that each disc of brine is surrounded by a "corona" of ice, with outer radius r_i. Then the minimal separation of brine inclusions is $2(r_i - r_b)$. Such a medium is called a $q-$material, where $q = r_b/r_i$. For such a geometry, Bruno has calculated [11]

$$s_m = \frac{1}{2}(1 - q^2), \qquad s_M = \frac{1}{2}(1 + q^2). \tag{3.10}$$

Smaller q values indicate well separated brine (and presumably cold temperatures), and $q = 1$ corresponds to no restriction on the separation, with $s_m = 0, s_M = 1$, so that R_1^{mp} and R_2^{mp} reduce to R_1 and R_2. Examination of photomicrographs of the brine microstructure in the sea ice samples of [2] indicates that even when the ice is quite cold, with brine volumes below the percolation threshold $p_c \approx 5\%$, corresponding to a critical temperature $T_c \approx -5°C$ at salinity 5 ppt, the brine inclusions are quite close, and it is very difficult to estimate appropriate values of q. Instead, for a given data set at a particular temperature, we choose a value of q which best captures the data, and it is always quite close to 1. (Computationally we find that because of the high contrast in the components, the bounds R_1^{mp} and R_2^{mp} are extremely sensitive to small changes in q for q near 1.) By carefully

comparing our bounds to data over a wide range of temperatures, we have found that as the temperature increases, i.e. as the percolation threshold T_c is approached and the brine inclusions grow closer, the data sweep across from one side of the region R_2 to the other (while the regions becomes larger as the brine volume increases), and q increases as well. Once the temperature is above T_c, the data require that $q = 1$, and the matrix-particle assumption is no longer valid. This fascinating behavior is illustrated in Figure 2, which compares data from samples 84-3 and 84-4 (S=3.8 ppt) in [2] with the bounds as the temperature is varied over a wide range. We remark that above the critical temperature, the brine phase becomes connected, and the sea ice is permeable, allowing percolation of brine, sea water, nutrients, biomass, and heat through the ice. In the Antarctic, this transition in the fluid transport properties plays a particularly important role in snow-ice formation [1], in heat fluxes through the ice [53], mixing in the upper ocean, and in the life cycles of algae living in the sea ice [23]. Furthermore, brine percolation has significant implications for remote sensing of sea ice, such as affecting its dielectric properties as above, and allowing flooding of the surface, which can alter microwave signatures [41, 54]. In [33], the striking similarity of sea ice microstructure to that of compressed polymer/metal powders [45] is exploited to provide a theoretical prediction of the critical brine volume of sea ice via percolation theory, and the geophysical and biological implications of brine percolation are explored.

4 Analytic wave theory for multilayer random media

For the interpretation of geophysical remote sensing data, analytic wave theory [94] has been used to develop scattering models for heterogeneous layered media such as sea ice. It is based on the vector wave equation

$$\nabla\times\nabla\times\mathbf{E} - k^2\epsilon(\mathbf{x})\mathbf{E} = \mathbf{0}, \tag{4.1}$$

where $k = \omega/c$ is the free space wave number. By writing the local complex permittivity $\epsilon(\mathbf{x})$ in terms of a constant, reference permittivity ϵ^0 and fluctuations $\zeta(\mathbf{x})$ about it,

$$\epsilon(\mathbf{x}) = \epsilon^0 + \zeta(\mathbf{x}), \tag{4.2}$$

then (4.1) can be converted to an integral equation

$$\mathbf{E}(\mathbf{x}) = \mathbf{E}^0 + k^2 \int d\mathbf{x}' \mathbf{G}^0(\mathbf{x},\mathbf{x}')\zeta(\mathbf{x}')\mathbf{E}(\mathbf{x}'), \tag{4.3}$$

where $\mathbf{G}^0$ is the dyadic Green's function for the homogeneous medium with complex permittivity ϵ^0, and $\mathbf{E}^0$ is the solution of (4.1) with $\epsilon(\mathbf{x}) = \epsilon^0$. In analytic wave theory, there are two principal choices for the reference permittivity. The first is $\epsilon^0 = \langle\epsilon(\mathbf{x})\rangle$, the mean of $\epsilon(\mathbf{x})$. The second is $\epsilon^0 = \epsilon_q^*$, where ϵ_q^* is the effective medium theory approximation for the quasistatic effective permittivity. With $\epsilon^0 = \langle\epsilon(\mathbf{x})\rangle$, iteration of (4.3) starting with $\mathbf{E}(\mathbf{x}') = \mathbf{E}^0$ generates a Neumann series for $\mathbf{E}(\mathbf{x})$, and truncating it at first order yields the Born approximation. The associated Dyson equation for the mean field can also be treated with a similar type of expansion. Various approximation schemes are based on inclusion of certain types of terms in the expansion, such as the bilocal approximation, which includes

those conributions from higher order terms which can be written in terms of products of bilocal (two-point) diagrams. Approximations based on the choice of $\epsilon^0 = \langle\epsilon\rangle$ are valid for small fluctuations $\zeta(\mathbf{x})$. However, for media such as sea ice, where these fluctuations can be quite large, it is more productive to choose $\epsilon^0 = \epsilon_q^*$, which leads to strong fluctuation theory. The singular nature of the dyadic Green's function is taken into account, and the bilocal approximation of (4.3) for an auxiliary field, or its Dyson equation, is used to approximate the scattering coefficients and the effective complex permittivity (including scattering effects). This theory is most accurate when the system is near the quasistatic regime, as it is, roughly speaking, an expansion about the quasistatic case, while the local fluctuations in $\epsilon(\mathbf{x})$ may be large.

Layered medium models have been developed with the Born approximation for an isotropic two-layer [99], isotropic multi-layer [100], anisotropic two-layer [51], or isotropic-anisotropic three-layer configurations [7] to calculate radar power returns or conventional backscattering coefficients. For polarimetric remote sensing, Mueller and covariance matrices which characterize fully polarimetric scattering properties of the media are calculated for an isotropic two-layer [9] or an anisotropic two-layer configuration [8]. In isotropic media containing spherical scatterers, depolarization giving rise to the cross polarization return is due to the second and higher order terms (multiple scattering) [9, 102]. However, stronger depolarization effects can come from the first-order term (single scattering) for anisotropic media [51, 8], or for non-spherical scatterers [65].

For dense media, the distorted Born approximation is applied [18, 76, 48, 48]. This approximation takes into account dissipation, scattering losses, and also the modification of the wave speed due to embedded scatterers. In this case, multiple scattering has been considered to some extent. Physically, the first order distorted Born approximation describes the single scattering process of the mean field, and can be interpreted as a first-order multiple scattering process. Further improvement has been obtained with a renormalization technique, which has been carried out to first order [25], second order [90], and higher order for a half-space isotropic random medium [15]. For a two-layer anisotropic medium, renormalization has been applied to derive the Dyson equation for the mean field and the Bethe-Salpeter equation for the scattered field, which are solved, respectively, under the nonlinear and the ladder approximations [49].

For media with strong variations in the permittivity, strong fluctuation theory [92] is used in conjunction with the distorted Born approximation, which is what is used here. Effective permittivities for isotropic and anisotropic random media have approximated with strong fluctuation theory [92, 82]. Scattering coefficients are then calculated under the distorted Born approximation with these effective permittivities [93, 91, 43, 64]. With a knowledge of the scattering coefficients, the emissivity of the ice can be determined using Kirchhoff's radiation law [73]. For sea ice, the brine inclusions are usually small compared to a wavelength in the microwave frequency range and have a permittivity distinctively higher than that of the background ice; thus strong fluctuation theory is particularly suitable.

An important advantage of analytic wave theory is the preservation of phase information. Since it is derived from wave equations for layered media with the use of dyadic Green's functions [99, 101, 50], wave theory solutions contain all multiple interactions due to the boundaries at the layer interfaces; therefore, all coherent effects for wave propagation in different directions such as constructive and destructive interferences are included.

To accurately model electromagnetic wave scattering in sea ice, it is necessary to consider the realistic complexity of sea ice and to define domains of model input parameters constrained by the sea ice physics. Sea ice is an inhomogeneous medium composed of an ice background, brine inclusions, air bubbles, and solid salt. The electromagnetic properties of these constituents are characterized by permittivities and permeabilities, which relate material characteristics to electromagnetic fields by constitutive relations. Except for air bubbles, the sea ice constituents such as seawater brine and pure ice are dispersive with large variations especially in the imaginary part of the permittivity as a function of wave frequency [21, 87].

Ice crystallographic structure determines the anisotropy of sea ice. Depending on the orientation distribution of the crystallographic c-axes, with an associated orientation distribution of layers of brine inclusions, sea ice can effectively be isotropic, uniaxial, or biaxial. The electromagnetic properties of sea ice are strongly related to the temperature, salinity, and density. These parameters together govern the thermodynamic phase distribution of sea ice constituents [17]. Surface roughness and surface conditions such as frost flowers, slush layer, hummocks, and snow characteristics (grain size, density, thickness) also impact the scattering from sea ice. Details of sea ice characteristics and their effects on electromagnetic properties can be found in [67].

4.1 Strong fluctuation theory for the effective complex permittivity of sea ice at microwave frequencies

The application of analytic wave theory to sea ice, and in particular the distorted Born approximation, depends upon being able to account for the strong permittivity fluctuations encountered in sea ice. Here we consider strong fluctuation theory for the effective complex permittivity. The sea ice is represented in general as a three component random mixture consisting of the three phases: pure ice, brine, and air. The description of sea ice as a random medium has been verified by statistical studies of random spatial variations in ice salinity and bubble distribution [96, 74, 71]. The ice is frequently also anisotropic due to the presence of brine inclusions that can have a much greater vertical than horizontal extent. In a general random medium, the local value of the permittivity at any point $\mathbf{x}$ is described by the random permittivity tensor $\epsilon(\mathbf{x})$. The definition of this tensor at a particular location depends on the complex permittivity at that location and the local geometry. The permittivity fluctuations are assumed to be statistically homogeneous. Strong fluctuation theory provides a consistent solution for both the effective permittivity, accounting for scattering losses, and the propagation of electromagnetic fields in the medium in terms of the spatial correlation functions of the components. We begin with consideration of the theory for a general random medium, and then present results arising from the detailed assumptions of the most recent models of sea ice.

In strong flutuation theory for a random medium [92, 81, 85, 65], the bilocal approximation is used to obtain the following analog of (4.1) for the mean electric field $\mathbf{E}^m$ propagating in the medium,

$$\nabla \times \nabla \times \mathbf{E}^m - k^2 \epsilon^* \mathbf{E}^m = 0, \tag{4.4}$$

where ϵ^* is the effective permittivity tensor in strong fluctuation theory, given by

$$\epsilon^* = \epsilon_q^* + \epsilon_s^*. \tag{4.5}$$

In (4.5), ϵ_q^* is the quasistatic permittivity tensor that describes the propagation of the electric field in an effective medium without volume scattering effects, which is discussed further below, and

$$\epsilon_s^* = k^2 \langle \boldsymbol{\xi} \mathbf{G} \boldsymbol{\xi} \rangle \tag{4.6}$$

is the contribution due to scattering from inhomogeneities. In (4.6), $\mathbf{G}$ and $\boldsymbol{\xi}$ are defined as follows. The dyadic Green's function $\mathbf{G}_q$ associated with the medium of constant permittivity ϵ_q^* satisfies

$$\nabla \times \nabla \times \mathbf{G}_q - k^2 \epsilon_q^* \mathbf{G}_q = \mathbf{I} \delta(\mathbf{x} - \mathbf{x}'), \tag{4.7}$$

where $\mathbf{I}$ is the unit dyad and δ is the Dirac delta function. $\mathbf{G}_q$ can be decomposed as

$$\mathbf{G}_q(\mathbf{x}, \mathbf{x}') = \mathbf{G}_q'(\mathbf{x}, \mathbf{x}') + \mathbf{S} \delta(\mathbf{x} - \mathbf{x}'), \tag{4.8}$$

where $\mathbf{G}_q'$ is the principal value of $\mathbf{G}_q$. $\mathbf{G}$ is the integral operator defined by convolution with $\mathbf{G}_q'$. The random tensor $\boldsymbol{\xi}$ in (4.6) is defined by

$$\boldsymbol{\xi}(\mathbf{x}) = \boldsymbol{\zeta}(\mathbf{x}) [\mathbf{I} - k^2 \mathbf{S} \boldsymbol{\zeta}(\mathbf{x})]^{-1}, \tag{4.9}$$

which is determined by the local fluctuations $\boldsymbol{\zeta}(\mathbf{x}) = \boldsymbol{\epsilon}(\mathbf{x}) - \epsilon_q^*$ and the delta function coefficient $\mathbf{S}$ of the dyadic Green's function.

The quasistatic effective permittivity tensor ϵ_q^* is chosen such that the mean value of $\boldsymbol{\xi}(\mathbf{x})$ is zero [92],

$$\langle \boldsymbol{\xi}(\mathbf{x}) \rangle = \mathbf{0}. \tag{4.10}$$

This condition removes secular terms in the diagrammatic expansion of an appropriate version of (4.1) for the auxiliary field $\mathbf{F} = (\mathbf{I} - k^2 \mathbf{S} \boldsymbol{\zeta}) \mathbf{E}$. For the special case of scalar local and effective permittivity, and a spherically symmetric correlation function so that $\mathbf{S} = (-1/(3k^2 \epsilon_q^*)) \mathbf{I}$, then [94]

$$\xi(\mathbf{x}) = 3\epsilon_q^* \left(\frac{\epsilon(\mathbf{x}) - \epsilon_q^*}{\epsilon(\mathbf{x}) + 2\epsilon_q^*} \right) \tag{4.11}$$

Then the condition (4.10) for n-component media with constituent complex permittivities $\epsilon_1, \epsilon_2, ..., \epsilon_n$ in the volume fractions $p_1, p_2, ..., p_n$, takes the form

$$\sum_{i=1}^{n} \frac{\epsilon_i - \epsilon_q^*}{\epsilon_i + 2\epsilon_q^*} p_i = 0 \tag{4.12}$$

The resulting expression for ϵ_q^* is the Polder and van Santen mixing formula [75], which is equivalent to Bruggeman's effective medium theory approximation for ϵ_q^* [10, 44, 47]. It should be remarked that a limitation of strong fluctuation theory is that the quasistatic limit ϵ_q^* as $k \longrightarrow 0$ of the effective complex permittivity in (4.5) is not the actual value considered rigorously in section 3 above, but is the effective medium *approximation*, which does not accurately capture the actual behavior of many random media. For example, while effective medium theory yields a percolation threshold for high contrast media, the resulting critical exponents describing effective transport near the threshold are incorrect.

Now, the scattering contribution to (4.5) is assumed to be that from an unbounded random medium and we ignore boundary effects. It is calculated using

$$\epsilon^*_{sil} = k^2 PV \int d^3\mathbf{x}'\, C_{ijkl}(\mathbf{x},\mathbf{x}') G'_{qjk}(\mathbf{x},\mathbf{x}') \exp[-i\mathbf{k}\cdot(\mathbf{x}-\mathbf{x}')], \tag{4.13}$$

where we have used the summation convention for repeated indices, PV denotes principal value, and C_{ijkl} is the correlation function of the permittivity fluctuations defined by

$$C_{ijkl}(\mathbf{x},\mathbf{x}') = \langle\, \xi_{ij}(\mathbf{x})\overline{\xi_{kl}(\mathbf{x}')}\,\rangle, \tag{4.14}$$

where the overbar denotes complex conjugation. The validity of equation (4.13) requires that the electric field does not oscillate too strongly over the volume where the kernel of the integral is significant, which effectively means that the correlation lengths should not be larger than the wavelength. For sea ice this approximation is sufficiently accurate for wavelengths greater than a few millimeters. The tensor $\mathbf{S}$ is the key to strong fluctuation theory. It takes into account explicitly the delta function part of $\mathbf{G}_q$ and allows the effects of rather large permittivity differences, such as those between ice, brine, and air to be incorporated accurately.

The application of the above formulation to the development of a particular model requires the following steps: [a] determine $\mathbf{S}$ based on the geometry of the inhomogeneities; [b] determine ϵ^*_q using equation (4.10); [c] determine the components of $\mathbf{G}_q$ and $\mathbf{G}'_q$ using (4.7) and (4.8); [d] determine C_{ijkl} from (4.14); and [e] calculate ϵ^*_s from (4.13). In practice this process is quite complex and the details differ significantly depending on the model used. For specific details, the reader is referred to the references.

Before proceeding to individual models, we note that if the correlation statistics of the medium have azimuthal symmetry about the vertical axis then the form of the permittivity can be simplified somewhat. In particular ϵ^*_q and $\mathbf{S}$ will be diagonal, and ϵ^* is symmetric [85] but can have off-diagonal components:

$$\epsilon^* = \begin{bmatrix} \epsilon^*_{11} & 0 & \epsilon^*_{13} \\ 0 & \epsilon^*_{11} & 0 \\ \epsilon^*_{13} & 0 & \epsilon^*_{33} \end{bmatrix}. \tag{4.15}$$

The component ϵ^*_{13} arises from the tilt of the inhomogeneities away from vertical and for the case of no tilt it will be zero. Further, if the statistics are locally isotropic, as for snow or frazil ice where the crystal structure is jumbled, we have the further simplification that $\epsilon^* = \epsilon^* \mathbf{I}$.

In order to model arctic sea ice, we assume that the system consists of a set of homogeneous layers of snow and saline ice. Both snow and ice layers are random mixtures of pure ice, brine, and air, whose permittivities are known functions of frequency and temperature. The appropriate values are reviewed in [38]. Each type of mixture is subject to constraints imposed by observed structural properties including the volume fractions, shapes and orientations of each constituent, and these constraints depend on ice type.

For the case of **snow**, the ice grains are assumed to be oriented isotropically in a discrete layer or layers on top of the ice. The structure in each snow layer is also assumed to be homogeneous. The snow may contain liquid at temperatures of 0°C and below when brine

is transported upward by capillary action from the underlying ice. Brine is commonly found in the snow on first-year ice [36, 52]. Stogryn [84] represents wet snow as an assembly of ice grains where the water is distributed in pendular rings at grain contact points and in thin films surrounding the grains. The fraction of water in the film around the ice grains is estimated to be (0.261-0.724 p_{water}), where p_{water} is the water volume fraction. He assumes that the correlation functions are exponential with correlation lengths

$$\begin{aligned} \ell_{ice} &= \frac{2}{3}(1-p_{ice})d_{grain}, \quad \ell_{film} = \ell_{ice}, \\ \ell_{rings} &= 0.54(1-p_{waterfilm})(p_{waterfilm}/p_{ice+waterfilm})^{0.5}d_{grain} \end{aligned} \tag{4.16}$$

Recent work by Mätzler [56] shows that, because the ice grains quickly undergo metamorphism and become distorted, it is more accurate to use $\ell_{ice} = \frac{2}{3}d_{grain}$. At centimeter and long millimeter wavelengths the effective permittivity is not very sensitive to the choice of ℓ_{ice}. Representative results from [84] are shown in Figures 3 (a) and (b). Rather close agreement is obtained between theory and observation for both real and imaginary parts of the permittivity. Note that for this data set, particular care was taken to determine the liquid water content of the snow samples.

For dry snow, Zurk *et al.* [103, 104] have taken into account the effects resulting from the tendency of snow grains to cluster. They find that clustering does not significantly affect $\mathrm{Re}(\epsilon^*)$ but it increases $\mathrm{Im}(\epsilon^*)$ significantly. The amount of the increase depends on the fractional volume occupied by the ice grains and the degree of clustering, and is most significant for low volume fractions where the grain placement is less constrained. This model provides a realistic representation for the observed spatial distribution of grains in natural snowpacks.

The principal case of interest for **sea ice** is first year congelation ice where the ice occurs as groups of platelets packed together to form grains with brine inclusions embedded between the platelets. Bulk salinities can range from about 4 to greater than 15 ppt. The brine inclusions are in general elongated and tend to be oriented vertically, but they can be tilted away from vertical [46, 37]. Varying amounts of air bubbles are also present giving densities in the range 0.92 to 0.88 $\mathrm{Mg/m^3}$.

The model of Stogryn [85] assumes that sea ice is a three phase (ice, brine, vapor) random medium with azimuthal symmetry about a vertical axis, and that a prolate spheroidal correlation function describes the brine inclusions. The brine inclusions are assumed to be tilted from vertical at a mean angle θ_B so that ϵ^* has the form shown in (4.15). The brine volume is determined from the bulk salinity S and temperature T using the equations of Frankenstein and Garner [22]. Vapor is then determined from the bulk density and the inclusions are assumed to be spherical. They contribute only to the diagonal terms of ϵ^*. Figure 4 shows a comparison of calculated values of the real and imaginary parts of ϵ^*_{11} for sea ice at two different temperatures compared with the observations of [97]. In addition to the results for first year ice, the model also has representations for frazil ice and multiyear ice. For further details the reader is referred to [85]. Recently, the integrated formulation in [16] that relates the brine volume and vapor volume to S, T, and bulk density, has been incorporated; however, it produces only small changes in the results presented here.

A series of models has been developed by Nghiem *et al.* [65, 67, 68, 71] culminating in a multispecies, anisotropic medium with vertical anisotropy. They assume that the brine

pockets and vapor inclusions in sea ice are triaxial ellipsoids including spheroids and spheres as special cases. For sea ice, the ellipsoids are oriented with their longest axis vertically and have random azimuthal orientations. The resulting ϵ^* is of the form of equation (4.15) with $\epsilon^*_{13} = 0$. For snow, the grains are represented as randomly oriented ellipsoids for which ϵ^* is a scalar. They investigate in detail the effects of distributions of size, shape, orientation and phase of the brine and vapor inclusions.

Representative results showing a comparison with the observations of Arcone *et al.* [2] are shown in Figure 5. By including the effects of actual salinity and temperature variations combined with brine loss from the samples at the higher temperatures, they obtain good agreement over a wide range of temperatures.

The formulations of both Stogryn and Nghiem *et al.* represent the snow cover as an isotropic medium and take into account the anisotropy present in sea ice and the thermal processes associated with the evolution of the ice. The principal differences are in the tilt of the brine inclusions and assumption of ellipsoids versus spheroids. More subtle differences involve the precise shapes of the inclusions, which are unfortunately quite variable in actual sea ice and depend not only on the present state of the ice and snow but on their temporal evolution. Although no direct intermodel comparison has been made, each model produces reasonable values of both real and imaginary parts of the effective permittivities for actual values of brine volume and bubble density and realistic representations of the microstructure of the ice. We conclude that these models are useful for determining ϵ^* and have sufficient flexibility to incorporate improvements in our understanding of the physical properties of sea ice.

4.2 Distorted Born approximation for sea ice

We now present the scattering calculation for sea ice under the distorted Born approximation, assuming that the system consists of n layers, $n = 0, 1, ..., N$. For example, we may have $n = 0$ the upper half space of air, $n = 1$ the cover layer such as snow, $n = 2$ the sea ice layer, and $n = 3$ the lower half space of sea water. To account for the medium anisotropy, the effective permittivity in layer n is described by the tensor ϵ^*_n from strong fluctuation theory discussed in the previous section. A polarimetric radar or scatterometer can measure the backscattered field for all polarizations, including magnitude and phase. Ensemble averages of scattered field correlations are used to obtain the complete set of polarimetric backscattering coefficients. These coefficients constitute a covariance matrix or a Mueller matrix, characterizing polarimetric scattering properties of the layered medium [64]. Now, the scattered field intensity $\langle\, |\mathbf{E}^s(\mathbf{x})|^2 \,\rangle$ for $\mathbf{x}$ in the upper half space $n = 0$ is given by

$$\begin{aligned} \langle\, |\mathbf{E}^s(\mathbf{x})|^2 \,\rangle \;=\; & k^4 \sum_{n=1}^{N} \int_{V_n} d\mathbf{x}_n \int_{V_n} d\mathbf{x}'_n C_{njklm}(\mathbf{x}_n, \mathbf{x}'_n) \cdot \\ & [\, \langle G_{ij}(\mathbf{x}, \mathbf{x}_n) \rangle \, \langle F^i_k(\mathbf{x}_n) \rangle \,] \, \overline{[\, \langle G_{il}(\mathbf{x}, \mathbf{x}'n) \rangle \, \langle F^i_m(\mathbf{x}'n) \rangle \,]} \,, \end{aligned} \tag{4.17}$$

where $\langle \mathbf{G}(\mathbf{x}, \mathbf{x}_n) \rangle$ is the mean dyadic Green's function of the anisotropic, layered medium with $\mathbf{x}$ in layer $n = 0$ and $\mathbf{x}_n$ in layer n, $\langle \mathbf{F}^i \rangle$ is the mean incident field in the effective medium with complex permittivity tensor ϵ^*_n, V_n is the volume occupied by layer n, and $\mathbf{C}_n$ is the correlation function of the scatterers in layer n, defined in (4.14), with variance

γ_{njklm} (depending on the volume fractions and permittivities of the sea ice constituents). The summation convention for repeated indices has been used on the lower indices in (4.17). Implicit in (4.17) are averages involving the probability density function of scatterer orientation angles ψ_n and ϕ_n in layer n, as well as the probability density function of layer thicknesses. The angular probability density is determined by the crystallographic c-axis distribution. (The indices i, j, k, l, m in (4.17) may be considered as vectors indicating the relative orientation of the ellipsoidal scatterers in a given layer relative to the global coordinate system; see [70] for details.) The correlation function $\mathbf{C}_n$ can be written as

$$C_{njklm}(\mathbf{x}_n, \mathbf{x}'_n) = \int d\mathbf{k}\, \gamma_{njklm} \Phi_n(\mathbf{k}) \exp[-i\mathbf{k} \cdot (\mathbf{x}_n - \mathbf{x}'_n)], \tag{4.18}$$

where Φ_n is the Fourier transform of

$$R_n(\mathbf{x}) = \exp\left[-\left(\frac{x^2}{\ell_{nx}^2} + \frac{y^2}{\ell_{ny}^2} + \frac{z^2}{\ell_{nz}^2} \right)^{\frac{1}{2}} \right] \tag{4.19}$$

with correlation lengths ℓ_{nx}, ℓ_{ny}, and ℓ_{nz}, related to the effective size and shape of the scatterers [65]. The scattering correlation (4.17) accounts for the physical and structural properties of the anisotropic sea ice, wave interaction with the medium interfaces, and effects of the cover layer.

Polarimetric backscattering coefficients $\sigma_{\mu\tau\nu\kappa}$ are calculated from

$$\sigma_{\mu\tau\nu\kappa} = \lim_{r, A \to \infty} \frac{4\pi r^2}{A} \frac{\langle E_\mu^s \, \overline{E_\nu^s} \rangle}{E_\tau^i \, \overline{E_\kappa^i}}, \tag{4.20}$$

where the subscripts μ, ν, τ, and κ in the linear polarization basis can be h for horizontal polarization or v for vertical polarization, r is the distance from the radar, and A is the illuminated area. In the covariance matrix, the conventional backscattering coefficients $\sigma_{hh} \equiv \sigma_{hhhh}$, $\sigma_{vv} \equiv \sigma_{vvvv}$, and $\sigma_{hv} \equiv \sigma_{hvhv}$ are the diagonal elements. The cross-correlation coefficients are σ_{hhhv} and σ_{hvvv}. The co-polarized ratio is σ_{vv}/σ_{hh}, the cross-polarized ratio is σ_{hv}/σ_{hh}, and the complex correlation coefficient between the horizontal and vertical returns is $\rho = \sigma_{hhvv}(\sigma_{hh}\sigma_{vv})^{-1/2}$. Complex mathematical expressions of $\sigma_{\mu\tau\nu\kappa}$ for sea ice covered by media such as snow and frost flowers have been derived and can be found in [67, 65, 70].

The microwave emissivity e_a of the snow-ice system, where $a = h$ for horizontal polarization and $a = v$ for vertical polarization, can then be determined from the scattering coefficients as follows:

$$e_a(\mathbf{k}^i) = 1 - \left| R_a(\mathbf{k}^i) \right|^2 - \frac{1}{4\pi} \int_0^{2\pi} d\phi \int_0^{\pi/2} d\theta \sin\theta \left[\sigma_{ah}(\mathbf{k}^i, \mathbf{k}^s) + \sigma_{av}(\mathbf{k}^i, \mathbf{k}^s) \right], \tag{4.21}$$

where $\mathbf{k}^i$ is the incident wave propagation vector, $\mathbf{k}^s(\theta, \phi)$ is the scattered wave propagation vector in the direction specified by the polar angle θ and azimuthal angle ϕ, and R_a is the Fresnel reflection coefficient for a plane wave incident on the ice. The resulting brightness temperature measured near the surface including the contribution reflected from the sky is

given by

$$T_a(\mathbf{k}^i) = e_a(\mathbf{k}^i)T_{surf} + |R_a|^2 T_{sky}(\mathbf{k}^i) + \frac{1}{4\pi}\int_0^{2\pi} d\phi \int_0^{\pi/2} d\theta \sin\theta \left[\sigma_{ah}(\mathbf{k}^i, \mathbf{k}^s) + \sigma_{av}(\mathbf{k}^i, \mathbf{k}^s)\right] T_{sky}(\mathbf{k}^i) \,. \quad (4.22)$$

To take into account the vertical structural variations in the ice, a multiple layer formulation has been developed [80], where the properties of the medium are constant in each layer but can differ between layers. This formulation has been extended to strong fluctuation theory and applied to snow and sea ice [83]. Specification of the reflection coefficient R_a of the coherent mean field in the medium and the components of the dyadic Green's function are determined by solving certain Ricatti equations which involve the effective permittivity tensor. The correlation statistics of both ice and snow are assumed to have anisotropy with a vertical optic axis and azimuthal symmetry. This represents the observed physical properties of sea ice (with random distribution of c axes in the horizontal plane) extremely well and simplifies the problem sufficiently that only two Ricatti equations need to be solved to specify all the components of the dyadic Green's function. The scattered field correlation is determined as described above, making use of an appropriate version of equation (4.18) for this case.

Surface roughness also impacts wave scattering from sea ice. Natural interfaces in sea ice are rough with various length scales from large scale hummocks to small scale roughness. The lower interface such as the boundary between sea ice and water can also be rough. In the layered configuration, one must take into account the effects of wave-boundary interactions, differential propagation delay, and wave attenuation of ordinary and extraordinary characteristic wave types in the anisotropic layered media. Hummocks modulate the small-scale rough surface scattering. Assuming the hummock and the small scale roughness are statistically independent and stationary Gaussian processes, the total roughness profile is a convolution of the individual roughness profiles at different scales. This convolved profile is used to calculate the composite rough surface scattering subject to the medium and propagation effects in the multilayered configuration [67].

In the following, we present applications of the model to ground-based, airborne, and spaceborne radar data for sea ice. Figure 6 compares the theoretical calculations and measured results for a layer of bare sea ice grown during the Cold Regions Research and Engineering Laboratory Experiment in 1993 (CRRELEX 1993) [69]. The data are obtained by the Jet Propulsion Laboratory (JPL) ground-based polarimetric scatterometer operated at C-band (center frequency at 5 GHz). The comparisons are good for backscattering coefficients (Figure 6a) and for normalized polarization signatures (Figure 6b). Figure 7 is for snow-covered first year sea ice and multiyear sea ice with snow and hummocks in the Beaufort sea. The JPL airborne Synthetic Aperture Radar (SAR) data were obtained during the Beaufort Sea Flight Campaign in 1988 near 75° north latitude and 142° west longitude. The spaceborne SAR data for sea ice in the Arctic were measured by the first European Remote Sensing Satellite (ERS-1) for vertical polarization [68]. The model results compare well with both the spaceborne and airborne radar data.

In summary, the layered model for sea ice scattering accounts for the three phases present in sea ice, the orientation distribution of crystallographic c-axes, non-spherical geometry of brine pockets and other inhomogeneities, anisotropy of columnar ice, thickness

distribution in thin ice, a brine layer and snow cover, roughnesses at sea ice interfaces, and melt hummocks. The model compares well with measured data in general, and provides physical insights into sea ice signatures observed by remote sensors, in order to interpret the signature behavior and to assess the retrieval of important geophysical parameters of sea ice.

5 Radiative Transfer Theory for Multilayer Random Media

In microwave remote sensing of earth terrain, volume and rough surface scattering give the principal contributions to radar backscatter responses. For volume scattering, both the random medium model, in which the scattering effects are accounted for by introducing a randomly fluctuating permittivity, and the discrete scatterer model, where randomly positioned particles are used to represent the volume inhomogeneities, have been used to calculate the electromagnetic scattering [42, 94, 95, 24]. As for the contribution from rough surfaces, different methods have been applied over the years to study such scattering. For example, for slightly rough surfaces, where the RMS height is much smaller than the wavelength, the small perturbation method (SPM) is used. On the other hand, when the radius of curvature of the surface is large, the tangent plane approximation or Kirchhoff's method can be used [42, 94, 95, 24].

Radiative transfer (RT) theory has been applied extensively to model electromagnetic wave propagation and scattering in geophysical media [42, 94, 95, 24]. Even though the RT approach deals only with the intensities of waves and neglects their coherent nature, it accounts for multiple scattering and obeys energy conservation. The propagation characteristics of the Stokes parameters associated with the fields are governed by an integro-differential equation, the radiative trasfer equation, which involves the extinction matrix, describing the attenuation of the specific intensity due to absorption and scattering, and the phase matrix, characterizing the coupling of intensities in two different directions due to scattering. The RT theory has been applied to scattering problems with highly complex geometry. Flat or rough surface boundary conditions can be imposed at the interfaces of a multilayered structure, and the rough surface scattering effects can be included in the RT model.

We now consider a multilayer random medium with layers $n = 0, 1, ..., N$, as in Figure 1 with $N = 5$. Layers 0 and N are homogeneous half spaces representing air and sea water, with appropriate complex permittivities. Layers $1, ..., N-1$ have boundaries at $z = 0, z = -d_1, ..., z = -d_{N-1}$, with thicknesses $|d_n - d_{n-1}|$, and background permittivities ϵ_n^b. Each layer n contains M_n types of scatterers, where each type $j = 1, ..., M_n$ is described by its fractional volume p_{nj}^s, permittivity ϵ_{nj}^s, size a_{nj}, b_{nj}, c_{nj}, and orientation distribution. Each interface can be either flat or randomly rough, with the corresponding variance γ_n and correlation length ℓ_n describing the roughness. The RT formulation for a multilayer medium containing discrete ellipsoidal scatterers and the numerical technique for solving the RT equations are described in the following.

The specific intensity $\mathbf{I}_n(z, \theta, \phi)$ at height z for propagation in the (θ, ϕ) direction inside each scattering layer $n = 1, ..., N-1$, is described by the generalized radiative transfer

equation,

$$\cos\theta \frac{d}{dz}\mathbf{I}_n(\theta,\phi,z) = -\kappa_{en}(\theta,\phi)\mathbf{I}_n(\theta,\phi,z) + \int_{4\pi} d\Omega' \mathbf{P}_n(\theta,\phi;\theta',\phi')\mathbf{I}_n(\theta',\phi',z) \quad (5.1)$$

where $\mathbf{I}_n$, $\mathbf{P}_n$ and κ_{en} are the Stokes vector, the phase matrix, and the extinction matrix inside layer n, respectively. The Stokes vector $\mathbf{I}$ associated with a wave with electric field $\mathbf{E} = E_v\hat{v} + E_h\hat{h}$, where $\hat{v}$ and $\hat{h}$ denote orthogonal polarizations, is defined as

$$\mathbf{I} = \begin{bmatrix} I_v \\ I_h \\ U \\ V \end{bmatrix} = \frac{1}{\eta}\begin{bmatrix} \langle E_v\overline{E_v}\rangle \\ \langle E_h\overline{E_h}\rangle \\ 2Re\langle E_v\overline{E_h}\rangle \\ 2Im\langle E_v\overline{E_h}\rangle \end{bmatrix}, \quad (5.2)$$

where η is the characteristic impedance, and $\langle\ \rangle$ denotes the ensemble average ($\mathbf{I}$ here is not to be confused with the identity matrix). The energy transport can be interpreted in the following heuristic way. As the intensities propagate through an infinitesimal length $ds = dz/\cos\theta$, there is an attenuation κ_{en} due to both absorption and scattering loss, but they also get enhanced by the scattering from all other directions (θ',ϕ') into the direction of propagation (θ,ϕ). This coupling is characterized by the phase matrix $\mathbf{P}_n$, and accounted for in (5.1) through integration over the solid angle 4π.

The phase matrix $\mathbf{P}_n$ relates the Stokes vector associated with the incident field to the Stokes vector associated with the scattered field, and is obtained as follows. The scattering function matrix $\mathbf{F}(\theta_s,\phi_s;\theta_i,\phi_i)$ which maps the incident field $\mathbf{E}^i = (E_v^i, E_h^i)$ in direction (θ_i,ϕ_i) to the scattered field $\mathbf{E}^s = (E_v^s, E_h^s)$ in direction (θ_s,ϕ_s) is given by

$$\mathbf{F}(\theta_s,\phi_s;\theta_i,\phi_i) = \begin{bmatrix} f_{vv} & f_{vh} \\ f_{hv} & f_{hh} \end{bmatrix}, \quad (5.3)$$

where the scattering amplitudes f_{ij} are functions of the the shape and permittivity of the scatterer. The associated incident and scattered Stokes vectors are transformed via the 4×4 Stokes matrix $\mathbf{L}(\theta_s,\phi_s;\theta_i,\phi_i)$, whose components are functions of f_{vv}, f_{vh}, f_{hv}, and f_{hh} [94]. The phase matrix $\mathbf{P}(\theta_s,\phi_s;\theta_i,\phi_i)$ is obtained from $\mathbf{L}$ by incoherent averaging over the type, dimension and spatial orientation of the scatterers. For example, the phase matrix for a mixture of one species of ellipsoid is given by

$$\mathbf{P}(\theta_s,\phi_s;\theta_i,\phi_i) = n_o \int da \int db \int dc \int d\alpha \int d\beta \int d\gamma \cdot f(a,b,c,\alpha,\beta,\gamma)\mathbf{L}(\theta_s,\phi_s;\theta_i,\phi_i) \quad (5.4)$$

where n_o is the number of scatterer per unit volume, a, b, c are the length of the ellipsoid semi-major axis, α,β,γ are the Eulerian angles which describe the orientation of the ellipsoid, and $f(a,b,c,\alpha,\beta,\gamma)$ is the joint probability density function for the quantities $a,b,c,\alpha,\beta,\gamma$.

The total extinction matrix κ_e can be obtained by summing the scattering and absorption losses in the medium [94]. The components of this 4×4 matrix are functions of

$$M_{ij} = \frac{i2\pi n_o}{k^b}\langle f_{ij}(\theta,\phi;\theta,\phi)\rangle \quad (5.5)$$

where k^b is the wave number in the background medium, $i, j = v, h$, and $\langle\ \rangle$ denotes average over the orientation and size distribution of the scatterers, as in (5.4).

For a layer containing M_n different types of scatterers, each with its own size, orientation distribution and fractional volume, the phase matrix can be obtained by incoherent averaging over different scatterers. The total absorption and scattering loss matrices due to M_n type of scatterers can also be calculated by incoherent averaging of the matrices associated with each scatterer type.

The boundary conditions necessary to solve for the Stokes vector inside layer n are as follows. At interface n,

$$\begin{aligned}
\mathbf{I}_n(\pi-\theta,\phi,z=-d_{n-1}) &= \mathbf{R}^c_{n,n-1}(\theta,\phi)\mathbf{I}_n(\theta,\phi,z=-d_{n-1}) \\
&+ \int_0^{2\pi} d\phi' \int_0^{\frac{\pi}{2}} d\theta' \sin\theta'\ \mathbf{R}^i_{n,n-1}(\theta,\phi;\theta',\phi') \\
&\quad \cdot\mathbf{I}_n(\theta',\phi',z=-d_{n-1}) \\
&+ \mathbf{T}^c_{n-1,n}(\theta_{n-1},\phi_{n-1})\mathbf{I}_{n-1}(\pi-\theta_{n-1},\phi_{n-1},z=-d_{n-1}) \\
&+ \int_0^{2\pi} d\phi'_{n-1} \int_0^{\frac{\pi}{2}} d\theta'_{n-1} \sin\theta'_{n-1}\ \mathbf{T}^i_{n-1,n}(\theta,\phi;\theta'_{n-1},\phi'_{n-1}) \\
&\quad \cdot\mathbf{I}_{n-1}(\pi-\theta'_{n-1},\phi'_{n-1},z=-d_{n-1}) \qquad (5.6)
\end{aligned}$$

and at interface $n+1$,

$$\begin{aligned}
\mathbf{I}_n(\theta,\phi,z=-d_n) &= \mathbf{R}^c_{n,n+1}(\theta,\phi)\mathbf{I}_n(\pi-\theta,\phi,z=-d_n) \\
&+ \int_0^{2\pi} d\phi' \int_0^{\frac{\pi}{2}} d\theta' \sin\theta' \mathbf{R}^i_{n,n+1}(\theta,\phi;\theta',\phi') \\
&\quad \cdot\mathbf{I}_n(\pi-\theta',\phi',z=-d_n) \\
&+ \mathbf{T}^c_{n+1,n}(\theta_{n+1},\phi_{n+1})\mathbf{I}_{n+1}(\theta_{n+1},\phi_{n+1},z=-d_n) \\
&+ \int_0^{2\pi} d\phi'_{n+1} \int_0^{\frac{\pi}{2}} d\theta'_{n+1} \sin\theta'_{n+1}\ \mathbf{T}^i_{n+1,n}(\theta,\phi;\theta'_{n+1},\phi'_{n+1}) \\
&\quad \cdot\mathbf{I}_{n+1}(\theta'_{n+1},\phi'_{n+1},z=-d_n) \qquad (5.7)
\end{aligned}$$

where $n = 2, 3, \ldots, N$-2 and θ_{n-1} and θ_{n+1} are the elevation angles in the local coordinate system of layers n-1 and n+1, respectively, and are related to θ by Snell's law. The matrices $\mathbf{R}^c_{l,m}$, $\mathbf{R}^i_{l,m}$, $\mathbf{T}^c_{l,m}$, and $\mathbf{T}^i_{l,m}$ in (5.6) and (5.7) are the respective coherent reflection, incoherent reflection, coherent transmission, and incoherent transmission matrices for the boundary between regions l and m. For a slightly rough interface, the small perturbation method can be used to solve for these matrices [94].

The boundary conditions at interfaces 1 and N ($z = 0$ and $z = -d_{N-1}$) are slightly different and can be written as follows. For interface 1 we have,

$$\begin{aligned}
\mathbf{I}_1(\pi-\theta,\phi,z=0) &= \mathbf{R}^c_{10}(\theta,\phi)\mathbf{I}_1(\theta,\phi,z=0) \\
&+ \int_0^{2\pi} d\phi' \int_0^{\frac{\pi}{2}} d\theta' \sin\theta' \mathbf{R}^i_{10}(\theta,\phi;\theta',\phi') \\
&\quad \cdot\mathbf{I}_1(\theta',\phi',z=0) \\
&+ \mathbf{T}^c_{01}(\theta_0,\phi_0)\mathbf{I}_{0i}(\pi-\theta_0,\phi_0) \\
&+ \mathbf{T}^i_{01}(\theta,\phi;\theta_{0i},\phi_{0i})\mathbf{I}_{0i} \qquad (5.8)
\end{aligned}$$

and at interface N,

$$\begin{aligned}\mathbf{I}_{N-1}(\theta,\phi,z=-d_{N-1}) &= \mathbf{R}^{c}_{N-1,N}(\theta,\phi)\mathbf{I}_{N-1}(\pi-\theta,\phi,z=-d_{N-1}) \\ &+ \int_0^{2\pi} d\phi' \int_0^{\frac{\pi}{2}} d\theta' \sin\theta' \mathbf{R}^{i}_{N-1,N}(\theta,\phi;\theta',\phi') \\ &\cdot\mathbf{I}_{N-1}(\pi-\theta',\phi',z=-d_{N-1}) \end{aligned} \tag{5.9}$$

where θ_0 is related to θ by Snell's law.

Both iterative and discrete ordinate eigen-analysis methods have been used to solve the RT equations [94]. Details of these two techniques can also be found in [94]. The iterative method is appropriate for cases of small albedo where absorption is dominant. The discrete ordinate eigen-analysis method provides numerical solutions for more general scattering cases. The Stokes vector and the phase matrix are first expanded into a Fourier series in the azimuthal angle ϕ. Then, the set of integrals over ϕ are carried out analytically to eliminate the ϕ dependence in the RT equations. The resulting equations are further solved using the Gaussian quadrature method by discretizing the angular variable θ for each harmonic of ϕ. Finally, the RT equations are transformed into a set of coupled first-order differential equations with constant coefficients. This set of equations is thus solved using the eigen-analysis method by obtaining the eigenvectors and eigenvalues and by matching the boundary conditions.

For a plane wave incident in region 0, the incident intensity is given by

$$\mathbf{I}_{0i}(\pi-\theta_0,\phi_0) = \mathbf{I}_{0i}\delta(\cos\theta_0-\cos\theta_{0i})\cdot\delta(\phi_0-\phi_{0i}) \tag{5.10}$$

The scattered wave in region 0 can be calculated by using the following equation

$$\begin{aligned}\mathbf{I}_{0s}(\theta_0,\phi_0) &= \mathbf{R}^{c}_{01}(\theta_0,\phi_0)\mathbf{I}_{0i}(\pi-\theta_0,\phi_0) \\ &+ \mathbf{R}^{i}_{01}(\theta_0,\phi_0;\theta_{0i},\phi_{0i})\mathbf{I}_{0i} \\ &+ \mathbf{T}^{c}_{10}(\theta,\phi)\mathbf{I}_1(\theta,\phi,z=0) \\ &+ \int_0^{2\pi} d\phi' \int_0^{\frac{\pi}{2}} d\theta' \sin\theta' \mathbf{T}^{i}_{10}(\theta_0,\phi_0;\theta',\phi')\mathbf{I}_1(\theta',\phi',z=0) \end{aligned} \tag{5.11}$$

The backscattering coefficient is obtained as

$$\sigma_{\mu\tau}(\theta_{0i},\phi_{0i}) = 4\pi\cos\theta_{0i}\frac{I_{0s\mu}(\theta_{0i},\phi_{0i}+\pi)}{I_{0i\tau}(\pi-\theta_{0i},\phi_{0i})} \tag{5.12}$$

where μ,τ can be v for vertical or h for horizontal polarization, and the subscripts i and s denote the incident and scattered waves, respectively.

6 Conclusions

A number of advances in the forward theory of electromagnetic scattering from sea ice have been made. Significant refinements of existing methods, such as analytic wave theory and radiative transfer theory, have been developed through incorporation of realistic features of the sea ice system, and close integration with experiments. These forward models include

both volume and surface scattering, and account for important features of sea ice such as bulk anisotropy, its multilayer character with rough interfaces between the layers, and inclusion size and orientation distributions for brine and air. Alternative approaches which are new to the sea ice remote sensing literature have also been introduced. Analysis of the Helmholtz equation for idealized sea ice models has led to rigorous results which lay the foundation for further theoretical advances in both forward and inverse scattering for complex media, including unexpected generalizations of key theorems in Fourier analysis. A general bounding method from the mathematical theory of homogenization for composite materials has been applied to the effective complex permittivity of sea ice. Accounting for the microstructural feature that the brine phase is contained in separated inclusions for temperatures colder than the percolation threshold, has led to significant improvement in the bounding method itself. At present, the bounds apply only in the quasistatic case, where scattering from individual inclusions is negligible. The effective complex permittivity of sea ice in the scattering regime has so far been estimated only with strong fluctuation theory, which is most accurate in the weakly scattering regime, near the quasistatic case. While many questions concerning the interaction of electromagnetic waves with sea ice remain, and the above findings have opened up important new avenues for further research, nevertheless, the body of work presented here has deepened our understanding of how the physical properties of sea ice detemine its electromagnetic signature.

Acknowledgements

The authors wish to acknowledge the support of the Office of Naval Research. The work carried out at the University of Utah (KMG) was supported by grants N00014-93-10141 and N00014-94-10958. The work done at Rensselaer Polytechnic Institute (MC and DI) was supported by grant ********. Research done at the Massachusetts Institute of Technology (KHD and JAK) was sponsored by N00014-89-J-1107 and N00014-92-J-4098. The work carried out at the University of Texas (AKF) was supported by N00014-96-1-0517. The research carried out by the Jet Propulsion Laboratory, California Institute of Technology was sponsored by the Office of Naval Research through an agreement with the National Aeronautics and Space Administration. The work conducted at the University of Washington (JS and DPW) was supported by N00014-89-J-3132, N00014-90-J-1369, N00014-93-0295, and N00014-96-1-0266. Finally, the authors would like thank Charles Luther and Wen Masters of the Office of Naval Research, and Arthur Jordan, of the Naval Research Laboratory, for their warm and sustained support throughout the ARI.

References

[1] S. F. Ackley, V. I. Lytle, K. M. Golden, M. N. Darling, and G. A. Kuehn. Sea ice measurements during ANZFLUX. *Antarctic Journal of the U.S.*, 30:133–135, 1995.

[2] S. A. Arcone, A. J Gow, and S. McGrew. Structure and dielectric properties at 4.8 and 9.5 GHz of saline ice. *J. Geophys. Res.*, 91(C12):14281–14303, 1986.

[3] M. Avellaneda and A. Majda. Stieltjes integral representation and effective diffusivity bounds for turbulent transport. *Phys. Rev. Lett.*, 62:753–755, 1989.

[4] D. J. Bergman. The dielectric constant of a composite material–A problem in classical physics. *Phys. Rep. C*, 43:377–407, 1978.

[5] D. J. Bergman. Exactly solvable microscopic geometries and rigorous bounds for the complex dielectric constant of a two-component composite material. *Phys. Rev. Lett.*, 44:1285, 1980.

[6] D. J. Bergman. Rigorous bounds for the complex dielectric constant of a two–component composite. *Ann. Phys.*, 138:78, 1982.

[7] M. Borgeaud, J. A. Kong, and F. C. Lin. Microwave remote sensing of snow-covered sea ice. In *Proceeding of the IGARSS'86 Symposium*, pages 133–138, September 8-11 1986.

[8] M. Borgeaud, S. V. Nghiem, R. T. Shin, and J. A. Kong. Theoretical models for polarimetric microwave remote sensing of earth terrain. *Journal of Electromagnetic Waves and Applications*, 3(1), 1989.

[9] M. Borgeaud, R. T. Shin, and J. A. Kong. Theoretical models for polarimetric radar clutter. *Journal of Electromagnetic Waves and Applications*, 1(1):73–89, 1987.

[10] D. A. G. Bruggeman. Berechnung vershiedener physicalischer konstanten von heterogenen substanzen. *Annalen der Physik*, 22:636–679, 1935.

[11] O. Bruno. The effective conductivity of strongly heterogeneous composites. *Proc. R. Soc. London A*, 433:353–381, 1991.

[12] F. D. Carsey, R. G. Barry, and W. F. Weeks. Introduction. In F. D. Carsey, editor, *Microwave Remote Sensing of Sea Ice*, pages 1–7. American Geophysical Union, 1992.

[13] M. Cheney and D. Isaacson. Inverse problems for a perturbed dissipative half-space. *Inverse Problems*, 11:865–888, 1995.

[14] E. Cherkaeva and K. M. Golden. Inverse bounds on the brine volume of sea ice from complex permittivity data. In preparation.

[15] H. T. Chuah and H. S. Tan. A high order renormalization method for radar backscatter from a random medium. *IEEE Trans. Geosci. Remote Sens.*, 27(1):79–85, 1989.

[16] G. F. N. Cox and W. F. Weeks. Equations for determining the gas and brine volumes in sea-ice samples. *J. Glaciology*, 29, 1983.

[17] G. F. N. Cox and W. F. Weeks. Equations for determining the gas and brine volumes in sea-ice samples. *J. Glaciol.*, 29(12):306–316, 1983.

[18] D. A. de Wolf. Electromagnetic reflection from an extended turbulent medium: Cumulative forward-scatter single backscatter approximation. *IEEE Trans. Antennas Propagat.*, AP-19, 1974.

[19] A. Einstein. Eine neue bestimmung der moleküldimensionen. *Ann. Physik*, 19:289–306, 1906.

[20] J. L. Ericksen, D. Kinderlehrer, R. Kohn, and J.-L. Lions (eds.). *Homogenization and Effective Moduli of Materials and Media, IMA Volumes in Mathematics and its Applications, Vol. 1.* Springer-Verlag, New York, 1986.

[21] S. Evans. Dielectric properties of ice and snow – a review. *J. Glaciol.*, 5, 1965.

[22] G. Frankenstein and R. Garner. Equations for determing the brine volume of sea ice from -0.5^o to -22.9^o C. *J. Glaciology*, 6(48):943–944, 1967.

[23] C. H. Fritsen, V. I. Lytle, S. F. Ackley, and C. W. Sullivan. Autumn bloom of Antarctic pack-ice algae. *Science*, 266:782–784, 1994.

[24] A. K. Fung. *Microwave Scattering and Emission Models and Their Applications.* Artech House, MA, 1994.

[25] A. K. Fung and H. S. Fung. Application of first-order renormalization method to scattering from a vegetation-like half-space. *IEEE Trans. Geosci. Electron.*, GE-15, 1977.

[26] K. Golden. Bounds on the complex permittivity of a multicomponent material. *J. Mech. Phys. Solids*, 34(4):333–358, 1986.

[27] K. Golden. Bounds on the complex permittivity of sea ice. *J. Geophys. Res. (Oceans)*, 100(C7):13,699 – 13,711, 1995.

[28] K. Golden and G. Papanicolaou. Bounds for effective parameters of heterogeneous media by analytic continuation. *Comm. Math. Phys.*, 90:473–491, 1983.

[29] K. M. Golden. Critical behavior of transport in lattice and continuum percolation models. *Phys. Rev. Lett.*, 78:3935–3938, 1997.

[30] K. M. Golden. Critical behavior of transport in percolation-controlled smart composites. In V. V. Varadan and J. Chandra, editors, *Mathematics and Control in Smart Structures, SPIE Proceedings Vol. 3039*, pages 571–581. SPIE - The International Society for Optical Engineering, 1997.

[31] K. M. Golden. The interaction of microwaves with sea ice. In G. Papanicolaou, editor, *Wave Propagation in Complex Media, IMA Volumes in Mathematics and its Applications, Vol. 96*, pages 75 – 94. Springer – Verlag, 1997.

[32] K. M. Golden and S. F. Ackley. Modeling of anisotropic electromagnetic reflection from sea ice. *J. Geophys. Res. (Oceans)*, 86(C9):8107–8116, 1981.

[33] K. M. Golden, S. F. Ackley, and V. I. Lytle. Brine percolation in sea ice. In preparation.

[34] K. M. Golden, D. Borup, M. Cheney, E. Cherkaeva, M. S. Dawson, K. H. Ding, A. K. Fung, D. Isaacson, S. A. Johnson, , A. K. Jordan, J. A. Kong, R. Kwok, S. V. Nghiem, R. G. Onstott J. Sylvester, D. P. Winebrenner, and I. Zabel. Inverse electromagnetic scattering models for sea ice. In preparation for a special issue of *Trans. Geosci. Rem. Sens.*

[35] K. M. Golden, G. R. Grimmett, R. D. James, G. W. Milton, , and P. N. Sen (eds.). *Mathematics of Multiscale Materials, IMA Volumes in Mathematics and its Applications, Vol. 99.* Springer-Verlag, New York, in press.

[36] T. C. Grenfell. Surface-based passive microwave observations of sea ice in the bering and greenland seas. *IEEE Trans. Geosci. Rem. Sens.*, GE-24:378–382, 1986.

[37] T. C. Grenfell and J. C. Comiso. Multifrequency passive microwave observations of first-year sea ice grown in a tank. *IEEE Trans. Geosci. Rem. Sens.*, GE-24:826–831, 1986.

[38] M. Hallikainen and D.P.Winebrenner. The physical basis for sea ice remote sensing, chapter 3. In F. Carsey, editor, *Microwave Remote Sensing of Sea Ice, Geophysical Monograph 68*, pages 29–46. AGU Publications, 1992.

[39] M. Hallikainen and D. P. Winebrenner. The physical basis for sea ice remote sensing. In F. D. Carsey, editor, *Microwave Remote Sensing of Sea Ice*, pages 29–46. American Geophysical Union, 1992.

[40] Z. Hashin and S. Shtrikman. A variational approach to the theory of effective magnetic permeability of multiphase materials. *J. Appl. Phys.*, 33:3125–3131, 1962.

[41] A. R. Hosseinmostafa, V. I. Lytle, K. C. Jezek, S. P. Gogineni, S. F. Ackley, and R. K. Moore. Comparison of radar backscatter from Antarctic and Arctic sea ice. *J. Electromagnetic Appl.*, 9:421–438, 1995.

[42] A. Ishimaru. *Wave Propagation and Scattering in Random Media, Vols. I and II.* Academic Press, New York, 1978.

[43] Y. Q. Jin and J. A. Kong. Strong fluctuation theory for scattering, attenuation, and transmission of microwave through snowfall. *IEEE Trans. Geosci. Remote Sens.*, GE-23(5):754–760, 1985.

[44] W. Kohler and G. Papanicolaou. Some applications of the coherent potential approximation. In P. L. Chow, W. E. Kohler, and G. C. Papanicolaou, editors, *Multiple Scattering and Waves in Random Media*, pages 199–223. North-Holland, New York, 1981.

[45] R. P. Kusy and D. T. Turner. Electrical resistivity of a polymeric insulator containing segregated metallic particles. *Nature*, 229:58, 1971.

[46] R.A. Lake and E.L. Lewis. Salt rejection by sea ice during growth. *J. Geophys. Res.*, 75:583–597, 1970.

[47] R. Landauer. Electrical conductivity in inhomogeneous media. In J. Garland and D. Tanner, editors, *AIP Conference Proceedings #40*, pages 2–43. American Institute of Physics, 1978.

[48] R. H. Lang and J. S. Sidhu. Electromagnetic backscattering from a layer of vegetation: A discrete approach. *IEEE Trans. Geosci. Remote Sens.*, GE-21(1):62–71, 1983.

[49] . K. Lee and J. A. Kong. Electromagnetic wave scattering in a two-layer anisotropic random medium. *J. Optical Soc. Amer.*, 2:2171–2186, 1985.

[50] J. K. Lee and J. A. Kong. Dyadic green's functions for layered anisotropic medium. *Electromagnetics*, 3:111–130, 1983.

[51] J. K. Lee and J. A. Kong. Active microwave remote sensing of an anisotropic random medium layer. *IEEE Trans. Geosci. Remote Sens.*, GE-23(6):910–923, 1985.

[52] A. W. Lohanick and T. C. Grenfell. Variations in brightness temperature over cold first-year sea ice near tuktoyaktuk, northwest territories. *J. Geophys. Res.*, 91(C4):5133–5144, 1986.

[53] V. I. Lytle and S. F. Ackley. Heat flux through sea ice in the Western Weddell Sea: Convective and conductive transfer processes. *J. Geophys. Res.*, 101(C4):8853–8868, 1996.

[54] V. I. Lytle and K. M. Golden. Microwave backscatter measurements from first year pack ice in the eastern Weddell Sea. *Antarctic Journal of the U.S.*, 30:125–127, 1995.

[55] G. Dal Maso and G. Dell'Antonio (eds.). *Proceedings of the Second Workshop on Composite Media and Homogenization Theory*. World Scientific, Singapore, 1995.

[56] C. Mätzler. Private communication, 1996.

[57] C. Mätzler and U. Wegmüller. Dielectric properties of fresh–water ice at microwave frequencies. *J. Phys. D: Appl. Phys.*, 20:1623–1630, 1987.

[58] J. C. Maxwell. *Electricity and Magnetism*. Clarendon Press, 1873.

[59] G. W. Milton. Bounds on the complex dielectric constant of a composite material. *Appl. Phys. Lett.*, 37:300–302, 1980.

[60] G. W. Milton. Multicomponent composites, electrical networks and new types of continued fractions I, II. *Comm. Math. Phys.*, 111:281–327, 329–372, 1987.

[61] G. W. Milton, D. J. Eyre, and J. V. Mantese. Finite frequency range Kramers Kronig relations: bounds on the dispersion. *Phys. Rev. Lett.*, 1997, to be published.

[62] G. W. Milton and K. Golden. Representations for the conductivity functions of multicomponent composites. *Comm. Pure. Appl. Math.*, 43:647, 1990.

[63] W. Luis Mochán and Rubén Barrera (eds.). *Proceedings of the Third International Conference on Electrical Transport and Optical Properties of Inhomogeneous Media.* Elsevier, Amsterdam, 1994.

[64] S. V. Nghiem, M. Borgeaud, J. A. Kong, and R. T. Shin. Polarimetric remote sensing of geophysical media with layer random medium model. In J. A. Kong, editor, *Progress in Electromagnetics Research*, volume 3, pages 1–73. Elsevier, New Yor, 1990.

[65] S. V. Nghiem, R. Kwok, J. A. Kong, and R. T. Shin. A model with ellipsoidal scatterers for polarimetric remote sensing of anisotropic layered media. *Radio Sci.*, 28(5):687–703, 1993.

[66] S. V. Nghiem, R. Kwok, J. A. Kong, R. T. Shin, S. A. Arcone, and A. J. Gow. An electrothermodynamic model with distributed properties for effective permittivities of sea ice. *Radio Science*, 31:297–311, 1996.

[67] S. V. Nghiem, R. Kwok, S. H. Yueh, and M. R. Drinkwater. Polarimetric signatures of sea ice 1. Theoretical model. *J. Geophys. Res.*, 100(C7):13665–13679, 1995.

[68] S. V. Nghiem, R. Kwok, S. H. Yueh, and M. R. Drinkwater. Polarimetric signatures of sea ice 2. Experimental observations. *J. Geophys. Res.*, 100(C7):13681–13698, 1995.

[69] S. V. Nghiem, R. Kwok, S. H. Yueh, A. J. Gow, D. K. Perovich, C. C. Hsu, K. H. Ding, and J. A. Kong. Evolution in polarimetric signatures of thin saline ice under constant growth. *Radio Science*, 32(1):127–151, 1997.

[70] S. V. Nghiem, R. Kwok, S. H. Yueh, J. A. Kong, C. C. Hsu, M. A. Tassoudji, and R. T. Shin. Polarimetric scattering from layered media with multiple species of scatterers. *Radio Science*, 30:835–852, 1995.

[71] S.V. Nghiem, R. Kwok, J.A. Kong, R.T. Shin, S.A. Arcone, and A.J. Gow. An electrothermodynamic model with distributed properties for effective permittivities of sea ice. *Radio Science*, 31:297–311, 1996.

[72] J. A. Ogilvy. *Theory of wave scattering from random rough surfaces.* IOP Publishing Ltd., London, 1991.

[73] W. H. Peake. Interaction of electromagnetic waves with some natural surfaces. *IRE Trans. Antennas Propagat.*, AP-7:324–329, 1959.

[74] D. K. Perovich and A. J. Gow. A statistical description of the microstructure of young sea ice. *J. Geophys. Res.*, 96:16,943–16,95, 1991.

[75] D. Polder and J. H. van Santen. The effective permeability of mixtures of solids. *Physica*, 12:257–271, 1946.

[76] S. Rosenbaum and L. W. Bowles. Clutter return from vegetated areas. *IEEE Trans. Antennas Propagat.*, AP-22(2):227–236, March 1974.

[77] R. Sawicz and K. Golden. Bounds on the complex permittivity of matrix-particle composites. *J. Appl. Phys.*, 78:7240–7246, 1995.

[78] R. A. Shuchman and R. G. Onstott. Remote sensing of the polar oceans. In W. O. Smith, editor, *Polar Oceanography, Part A, Physical Science*, pages 123–169. Academic Press, 1990.

[79] E. Somersalo, M. Cheney, D. Isaacson, and E Isaacson. Layer stripping: a direct numerical method for impedance imaging. *Inverse Problems*, 7:899–926, 1991.

[80] A. Stogryn. Electromagnetic scattering by random dielectric constant fluctuations in a bounded medium. *Radio Sci.*, 9:509–518, 1974.

[81] A. Stogryn. The bilocal approximation for the electric field in strong fluctuation theory. *IEEE Trans. Anten. Prop*, AP-31(6):985–986, 1983.

[82] A. Stogryn. The bilocal approximation for the effective dielectric constant of an isotropic random medium. *IEEE Trans. Antennas Propagat.*, AP-32(5):517–520, 1984.

[83] A. Stogryn. A study of the microwave brightness temperature of sea ice, Aerojet General Report #8362. 1986.

[84] A. Stogryn. A study of the microwave brightness temperature of snow from the point of view of strong fluctuation theory. *IEEE Trans. Geosci. Remote Sens.*, GE-24:220–231, 1986.

[85] A. Stogryn. An analysis of the tensor dielectric constant of sea ice at microwave frequencies. *IEEE Trans. Geosci. Rem. Sens.*, GE-25(2):147–158, 1987.

[86] A. Stogryn and G. J. Desargant. The dielectric properties of brine in sea ice at microwave frequencies. *IEEE Trans. Antennas Propagat.*, AP-33(5):523–532, 1985.

[87] A. Stogryn and G. J. Desargent. The dielectric properties of brine in sea ice at microwave frequencies. *IEEE Trans. on Antennas and Propagat.*, AP-33(5):523–532, 1985.

[88] J. Sylvester and G. Uhlmann. A global uniqueness theorem for an inverse boundary value problem in electrical prospection. *Ann. Math.*, 125:153–169, 1987.

[89] J. Sylvester, D. Winebrenner, and F. Gylys-Colwell. Layer stripping for the helmholtz equation. *SIAM J. Appl. Math.*, 56:736–754, 1996.

[90] H. S. Tan, A. K. Fung, and H. Eom. A second-order renormalization theory for cross-polarized backscatter from a half space random medium. *Radio Sci.*, 15(6):1059–1065, 1980.

[91] L. Tsang and J. A. Kong. Application of strong fluctuation random medium theory to scattering from vegetation-like half space. *IEEE Trans. Geosci. Remote Sens.*, GE-19(1):62–69, January 1981.

[92] L. Tsang and J. A. Kong. Scattering of electromagnetic waves from random media with strong permittivity fluctuations. *Radio Sci.*, 16(3), 1981.

[93] L. Tsang, J. A. Kong, and R. W. Newton. Application of strong fluctuation random medium theory to scattering of electromagnetic waves from a half-space of dielectric mixture. *IEEE Trans. Antennas Propagat.*, 2AP-30:292–302, 1982.

[94] L. Tsang, J. A. Kong, and R. T. Shin. *Theory of Microwave Remote Sensing.* John Wiley and Sons, New York, 1985.

[95] F.T. Ulaby, R.K. Moore, and A.K. Fung. *Microwave Remote Sensing: Active and Passive, Vols. I, II and III.* Artech House, MA, 1986.

[96] F. Vallese and J. A. Kong. Correlation function studies for snow and ice. *J. Appl. Phys.*, 52:4921–4925, 1981.

[97] M. Vant, R. Ramseier, and V. Makios. The complex dielectric constant of sea ice at frequencies in the range 0.1 to 40 ghz. *J. Appl. Phys.*, 49:1264–1280, 1978.

[98] D. P. Winebrenner, J. Bredow, A. K. Fung, M. R. Drinkwater, S. Nghiem, A. J. Gow, D. K. Perovich, T. C. Grenfell, H. C. Han, J. A. Kong, J. K. Lee, S. Mudaliar, R. G. Onstott, L. Tsang, and R. D. West. Microwave sea ice signature modeling. In F. D. Carsey, editor, *Microwave Remote Sensing of Sea Ice*, pages 137–175. American Geophysical Union, 1992.

[99] M. Zuniga and J. A. Kong. Active remote sensing of random media. *J. Applied Phys.*, 51:4–79, 1980.

[100] M. A. Zuniga, T. M. Habashy, and J. A. Kong. Active remote sensing of layered random media. *IEEE Trans. Geosci. Electron.*, GE-17(4):296–302, 1979.

[101] M. A. Zuniga and J. A. Kong. Mean dyadic green's function for a two-layer random medium. *Radio Sci.*, 16(6), 1981.

[102] M. A. Zuniga, J. A. Kong, and L. Tsang. Depolarization effects in the active remote sensing of random media. *J. Applied Phys.*, 51(5), 1980.

[103] L. M. Zurk, K.H. Ding L. Tsang, and D.P. Winebrenner. Monte carlo simulations of the extinction rate of densely packed spheres with clustered and non-clustered geometries. *J. Opt. Soc. Amer.*, 12:1771–1781, 1995.

[104] L. M. Zurk, K.H. Ding L. Tsang, and D.P. Winebrenner. Scattering properties of dense media from monte carlo simulations with application to active remote sensing of snow. *Radio Science*, 31:803–819, 1996.

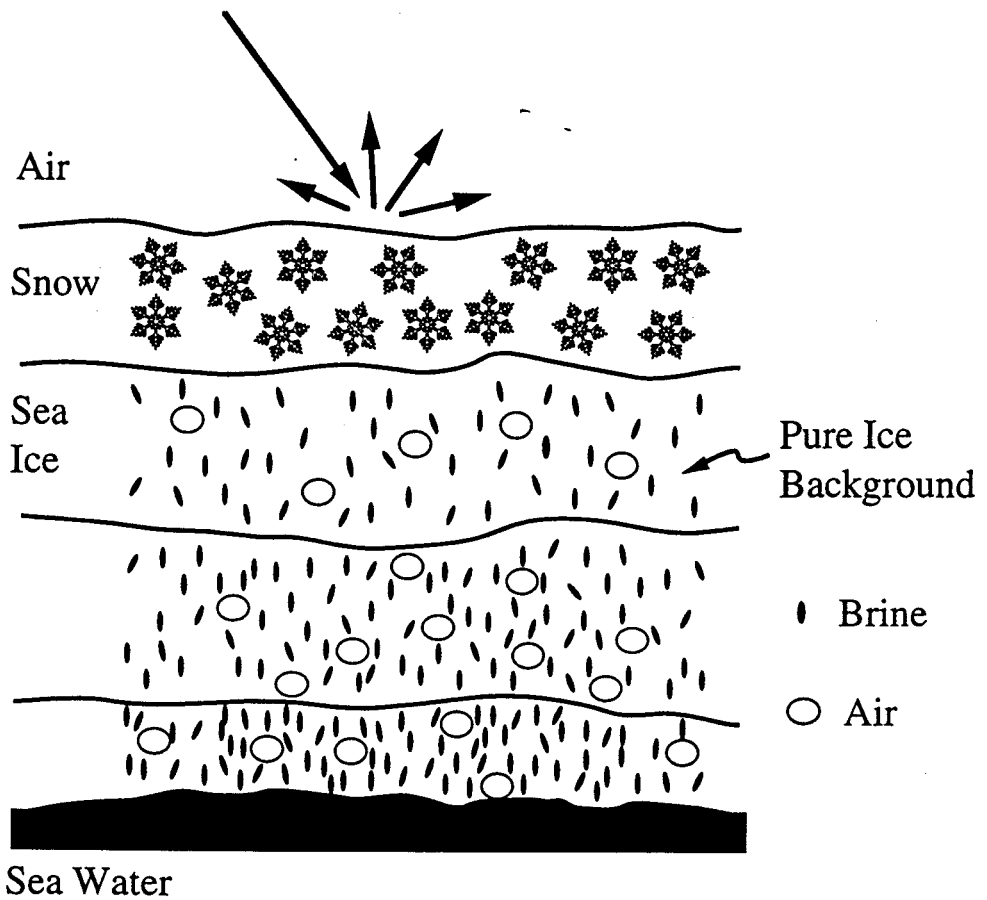

Figure 1: Multilayer random inclusion model for sea ice.

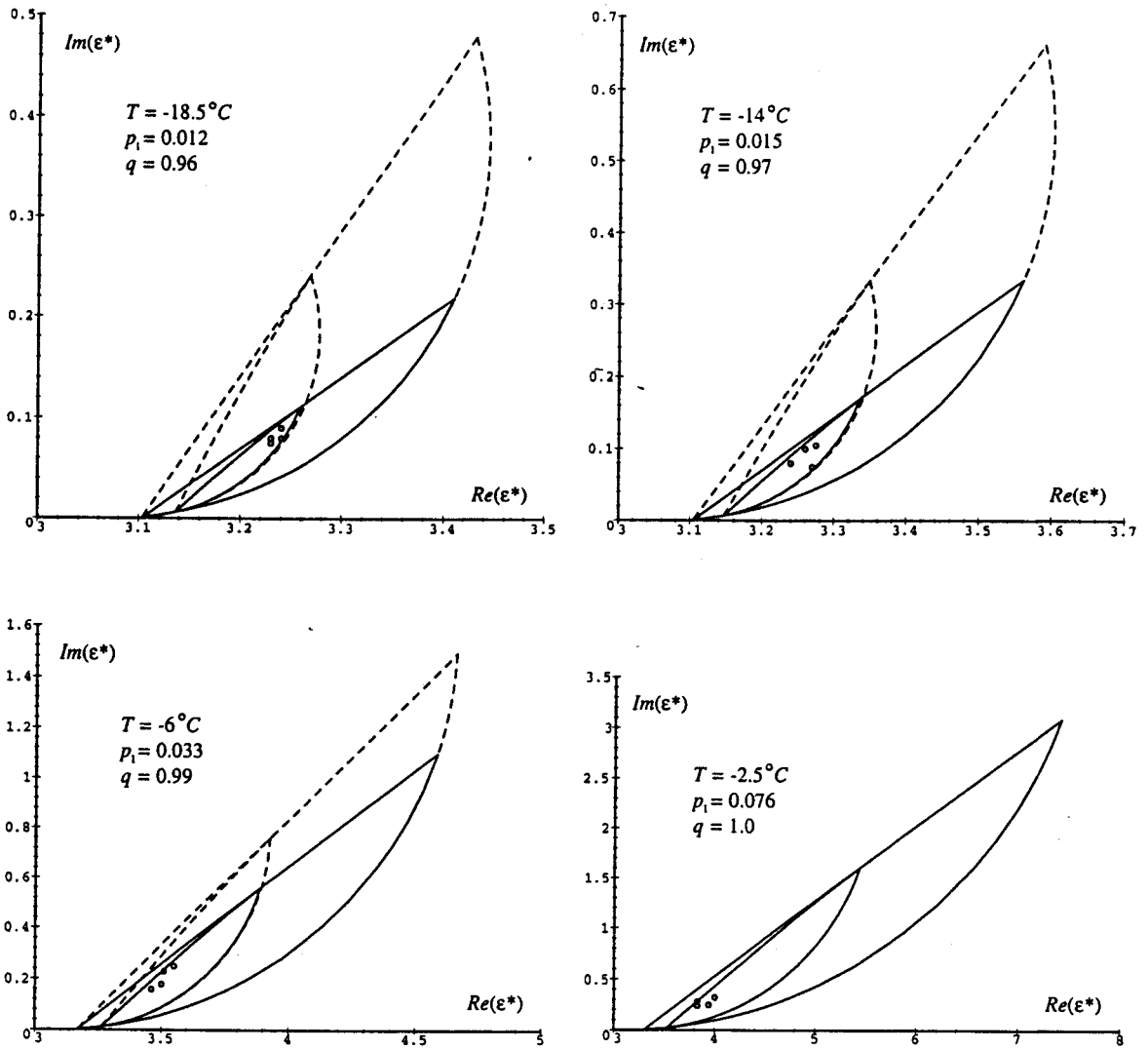

Figure 2: Comparison of 4.75 GHz data (circles) on the complex permittivity ϵ^* of sea ice at different temperatures with the bounds R_1 (outer, dotted), R_2 (inner, dotted), R_1^{mp} (outer, solid), and R_2^{mp} (inner, solid). R_1 assumes only knowledge of the brine volume and R_2 assumes statistical isotropy as well. R_1^{mp} and R_2^{mp} further assume that the sea ice is a matrix-particle composite with the q values indicated. Note that as the temperature increases, the data move across the region R_2 (while the regions become larger), and q increases, indicating decreased separation of the brine inclusions. For $T = -2.5°C$, which is above the percolation threshold, the matrix-particle assumption is no longer valid, so that $q = 1$, and R_1^{mp} and R_2^{mp} reduce to R_1 and R_2 .

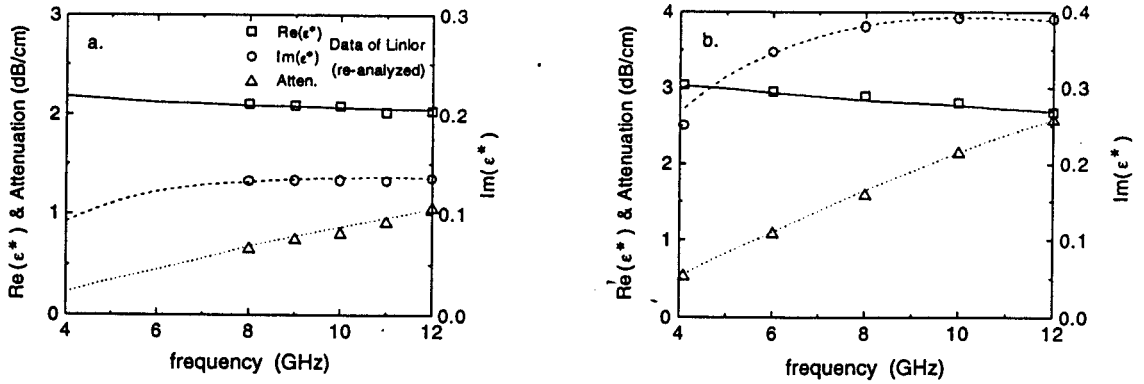

Figure 3: Calculated values of ϵ^* and attenuation for wet snow [solid and dotted lines] assuming $d_{grain} = 1$ mm. Case a, density = 0.442 Mg/m^3, $p_{water} = 0.251$. Case b, density = 0.558 Mg/m^3, $p_{water} = 0.624$. The open symbols denote the observations. Redrawn from [84].

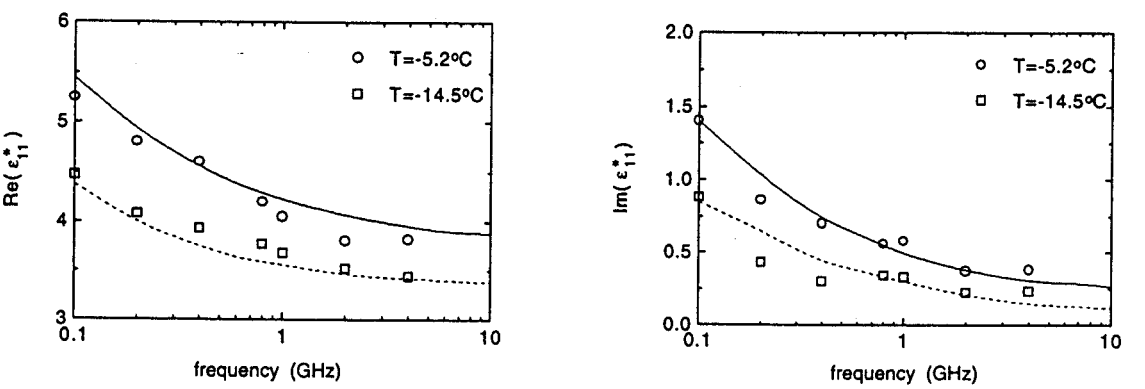

Figure 4: Calculated real and imaginary parts of ϵ^*_{11} for sea ice [solid and dotted lines] compared with the observations of Vant *et al.* [97] [circles and squares]. Ice salinity is 10.5 ppm, ice density is 0.91 Mg/m^3, $\theta_B = 24°$, and $\ell_\rho/\ell_z = 200$, where ℓ_ρ is the correlation length in the radial direction. Redrawn from [85].

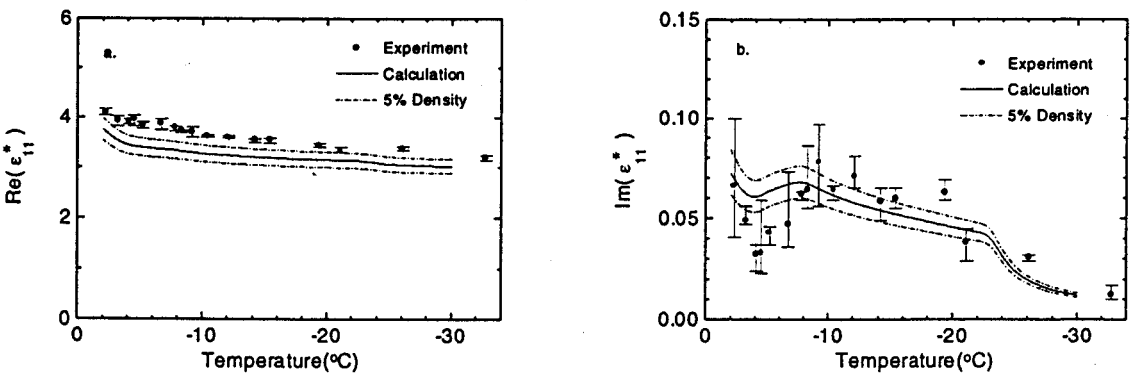

Figure 5: Effects of density differences on the (a) real and (b) imaginary parts of ϵ_{11}^* for young sea ice as a function of temperature for an extended warming sequence. The solid circles are the experimental results, the solid curve is for the calculated results, and the dash-dotted curves are for upper and lower bounds by varying the bulk ice density by $\pm 5\%$. Redrawn from [71].

(a) Backscatter Results

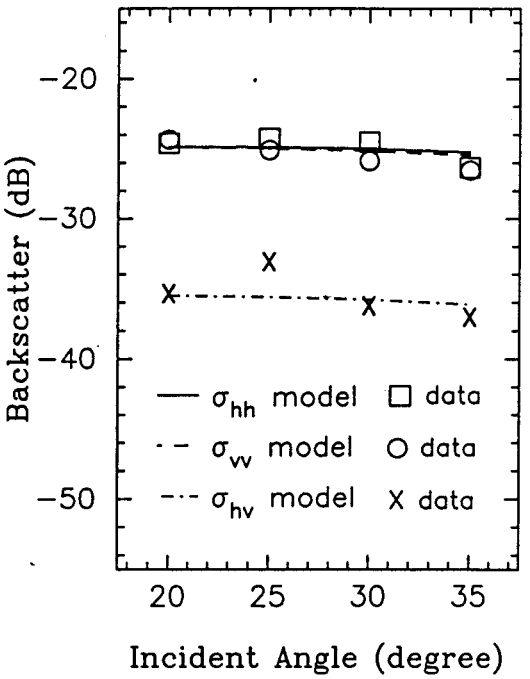

(b) Polarimetric Signatures

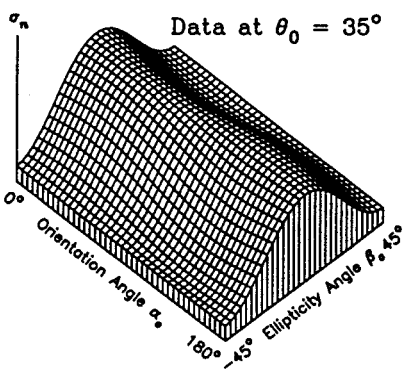

FIGURE 1b (Data)

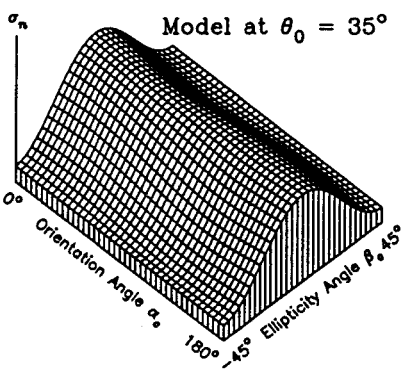

FIGURE 1b (Model)

Figure 6: Comparison of theoretical calculations based on the distorted Born approximation, to CRRELEX data on bare sea ice, for (a) backscatter coefficients and (b) polarimetric signatures.

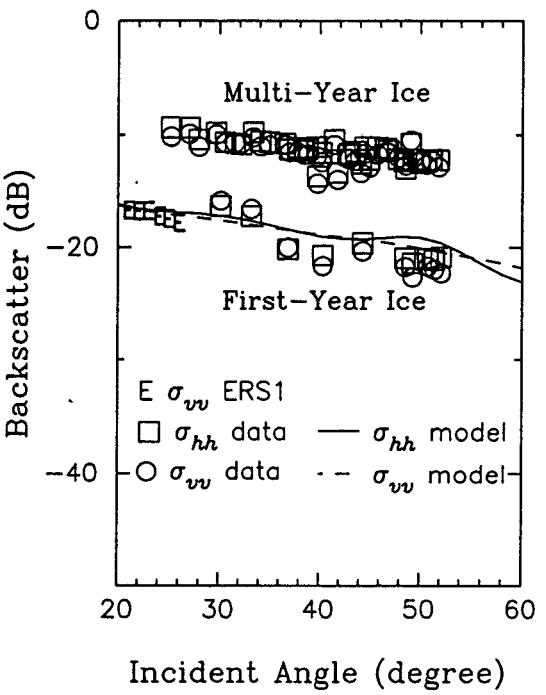

Figure 7: Comparison of theoretical calculations of backscatter based on the distorted Born approximation, to SAR data for snow-covered sea ice in the Beaufort Sea, measured by ERS-1 and during the Beaufort Sea Flight Campaign.